Fiber-Optic Parametric Amplifiers for Lightwave Systems

F. Yaman, Q. Lin, and Govind P. Agrawal

Institute of Optics, University of Rochester, Rochester, NY 14627

May 21, 2005

Abstract

Fiber-optic parametric amplifiers (FOPAs) can be used in lightwave systems for several signal-processing applications including optical amplification, phase conjugation, and wavelength conversion. In this review we focus on some of the recent advances in designing broadband FOPAs. The well-known simple theory behind the nonlinear phenomenon of four-wave mixing is discussed first to provide the background material. It is then used to discuss the performance of single-pump and double-pump FOPAs and reveal the important role played by the nonlinear contribution to phase matching. We discuss the design of dual-pump FOPAs and show how they can provide a gain spectrum that is relatively uniform over a bandwidth larger than 100 nm. We also study the impact of fluctuations in the zero-dispersion wavelength along the fiber length and show that fluctuations as small as ± 1 nm degrade severely the gain spectrum of FOPAs because they mainly affect its central flat part. This degradation can be avoided to a large extent by moving pump wavelengths closer. Birefringence fluctuations that occur in all practical fibers and lead to polarization-mode dispersion (PMD) also affect the gain spectrum of FOPAs. A vector theory based on the Jones-matrix formalism is developed for this purpose. We discuss how PMD affects the gain spectrum and make the FOPA gain polarization dependent even when orthogonally polarized pumps are used.

1 Introduction

Modern optical communication systems require not only signal amplification periodically but also devices that are capable of ultrafast, all-optical, signal processing. Fiber-optic parametric amplifiers (FOPA), based on four-wave mixing (FWM) occurring inside optical fibers [1], are attracting considerable attention because they can provide broadband amplification and can thus replace erbium-doped fiber amplifiers used commonly for signal amplification [2]–[6]. However, although not yet fully appreciated, FOPAs are also an ideal candidate for ultrafast, all-optical, signal processing because of an instantaneous electronic response of the silica nonlinearity responsible for FWM in optical fibers. Moreover, amplification provided by FOPAs is accompanied with relatively low noise, allowing operation close to the quantum limit.

Reasonably large values of optical gain with a relatively flat and wide gain spectrum can be realized when FOPAs are either pumped in the vicinity of zero-dispersion wavelength (ZDWL) using a single pump laser [1]–[3] or pumped using two lasers at two well-selected wavelengths located on each side of the ZDWL [4]–[6]. Such FOPAs have recently been used for applications such as broadband WDM amplification, wavelength conversion, optical sampling, and pulse compression [1]–[6]. A feature unique to FOPAs is that the idler field generated during signal amplification is phase-conjugated. Such phase conjugation provides an efficient way for dispersion compensation [7], as already demonstrated experimentally [8]. It can also be used to reduce timing jitter [9] as well as phase jitter [10] in long-haul lightwave systems. Although FOPAs can be used to manipulate quantum noise with a proper control of phase differences among the four interacting waves [11]–[13], modern communication systems do not yet employ phase-sensitive amplification.

In this chapter, we review the recent progress that has been realized in the field of FOPAs. Among many applications of such devices, we focus on signal amplification and wavelength conversion. We recall in Section 2 the basic theory behind the nonlinear phenomenon of FWM and use it in Section 3 to discuss the performance of single-pump FOPAs. Section 4 focuses on the more general case of dual-pump FOPAs and shows how the use of two pumps at suitable wavelengths can provide uniform gain over a wide bandwidth. Sections 5 and 6 discuss the impact of two major phenomena that affect the performance of all FOPA-based devices. The ZDWL of a fiber can vary along its length in a random fashion owing to core-diameter variations that occur invariably during fiber manufacturing; the effects of ZDWL fluctuations are discussed in Section 5. Section 6 then focuses on birefringence fluctuations that also occur in all practical fibers and lead to a phenomenon known as polarization-mode dispersion (PMD). The main results are summarized in the concluding section.

2 Theory of Four-Wave Mixing

The FWM process originates from the nonlinear response of bound electrons to intense optical waves inside nonlinear media such as silica fibers. When two intense pump waves at frequencies ω_1 and ω_2 copropagate inside an optical fiber, they can force the bound electrons to oscillate almost instantaneously at any frequency stemming from the mixing of these waves. Even though the potential provided by silica molecules confines electrons to their original atom, electrons respond to the applied electromagnetic field by emitting secondary waves not only at the original frequencies ω_1 and ω_2 (linear response), but also at two new frequencies denoted as ω_3 and ω_4 (third-order nonlinear response). Physically, two photons at the original frequencies are scattered elastically into two new photons at frequencies ω_3 and ω_4. The total energy and momentum of the original two photons are conserved during FWM. Noting that photon energy and momentum are $\hbar\omega$ and $\hbar\beta$, respectively, for an optical field of frequency ω propagating with the propagation constant β, the conservation relations take the form:

$$\omega_1 + \omega_2 = \omega_3 + \omega_4, \qquad \beta(\omega_1) + \beta(\omega_2) = \beta(\omega_3) + \beta(\omega_4), \tag{1}$$

where β is the propagation constant as a function of frequency. Only the magnitude of wave vectors appears in Eq. (1), because all four waves propagate along the same direction in single-mode fibers. Since $\beta(\omega_j)$ governs the phase shift experienced by the jth wave, second half of Eq. (1) is also referred to as the phase-matching condition [14].

A question that must be answered is what determines the frequencies ω_3 and ω_4 during the FWM process? If only the pump beams are incident on an optical fiber, the new waves grow from noise and their frequencies are determined by the phase-matching condition through spontaneous FWM. In practice, the efficiency of the FWM process is enhanced by seeding it. Seeding is accomplished by launching a signal wave at the frequency ω_3. The probability of creating photons at the frequency ω_4 depends on how many photons at ω_3 already exist inside the fiber. As a result, the FWM process is stimulated, and new photons at ω_3 and ω_4 are created with an exponential growth rate provided the phase-matching condition is nearly satisfied. It is common to refer to the fourth wave at the frequency ω_4 as the *idler wave*, following the terminology used in the microwave literature. It is not obligatory to launch two separate pump beams for FWM to occur. The same process can occur even when the two pump photons have the same frequency (degenerate FWM). The general case of two independent pump beams is called nondegenerate FWM.

Mathematically, the description of FWM is relatively simple for optical fibers since all four waves propagate in the form of a fiber mode and maintain their spatial profile [1]. Since they also propagate along the same fiber axis (assumed to coincide with the z axis), transverse effects can be completely ignored, and

one can use a one-dimensional model. Moreover, if we assume perfect cylindrical symmetry for optical fibers (no residual birefringence), and also assume that all waves are linearly polarized in the same direction we can employ the scalar approximation. We shall relax this approximation in Section 6 since silica fibers do exhibit some residual birefringence that changes randomly along the fiber length.

The FWM analysis is simplified considerably if we assume that the signal and idler powers remain relatively small throughout the fiber length compared with the pump powers. This amounts to assuming that pumps are not depleted during the FWM process. The evolution of the signal and idler waves is then governed by the following two coupled but linear equations [1]:

$$\frac{dB_3}{dz} = \frac{i}{2}\kappa B_3 + 2i\gamma B_1 B_2 B_4^*, \tag{2}$$

$$\frac{dB_4}{dz} = \frac{i}{2}\kappa B_4 + 2i\gamma B_1 B_2 B_3^*, \tag{3}$$

where $\kappa = \Delta\beta + \gamma(P_1 + P_2)$ describes the total phase mismatch and γ is the nonlinear parameter defined as $\gamma = 2\pi n_2/(\lambda_p A_{\text{eff}})$, where $n_2 \approx 2.6 \times 10^{-20}$ m^2/W is for silica fibers, λ_p is the average pump wavelength, and A_{eff} is the effective core area of the fiber. Also, $\Delta\beta = \beta(\omega_3) + \beta(\omega_4) - \beta(\omega_1) - \beta(\omega_2)$ is the linear phase mismatch resulting from fiber dispersion and P_1 and P_2 are the input powers of two pumps. The optical field amplitudes for the signal and idler waves, A_3 and A_4, are related to B_3 and B_4 by a phase factor through $A_j = B_j \exp\{iz[-\kappa/2 + 2\gamma(P_1 + P_2)]\}$. In Eqs. (2) and (3), we have included the contribution of self-phase modulation (SPM) and cross-phase modulation (XPM) induced by the two pumps, but these nonlinear effects originating from the signal and idler waves are neglected. Fiber losses are ignored because only a relatively short length of fiber ($\sim$ 1 km) is generally used for making FOPAs.

From Eqs. (2) and (3), the signal and idler powers, $P_3 = |B_3|^2$ and $P_4 = |B_4|^2$, are found to satisfy the same equation:

$$\frac{dP_3}{dz} = \frac{dP_4}{dz} = 2\xi\sqrt{P_3 P_4}\sin\theta, \tag{4}$$

where $\xi = 2\gamma\sqrt{P_1 P_2}$ is a measure of the FWM efficiency in the nondegenerate case and $\theta = \phi_3 + \phi_4 - \phi_1 - \phi_2$ describes the accumulated phase mismatch among the four waves. Here ϕ_j is the phase of the field B_j, i.e., $B_j = \sqrt{P_j}\exp(i\phi_j)$. When the two pumps are assumed to remain undepleted, ϕ_1 and ϕ_2 maintain their initial values, and the accumulated phase mismatch is governed by

$$\frac{d\theta}{dz} = \kappa + \xi\cos\theta\,\frac{(P_3 + P_4)}{\sqrt{P_3 P_4}}. \tag{5}$$

Equation (4) shows clearly that the growth of the signal and idler waves inside a fiber is determined by the phase-matching condition. When $\theta = \pi/2$, signal and idler extract energy from the two pumps. In contrast, when $\theta = -\pi/2$, energy can flow back to the two pumps from the signal and idler. If only the two pumps and

the signal are launched into FOPA initially, the idler wave is automatically generated by the FWM process. This can be seen from Eq. (3). Even if $B_4 = 0$ at $z = 0$, its derivative is not zero as long as $B_3(0)$ is finite. If we integrate this equation over a short fiber section of length Δz, we obtain $\Delta B_4 \approx 2i\gamma B_1 B_2 B_3^*(0)\Delta z$. The factor of i provides an initial value of $\pi/2$ for θ and shows that the correct phase difference is automatically picked up by the FWM process [15]. If $\kappa = 0$ initially (perfect phase matching), Eq. (5) shows that θ will remain frozen at its initial value of $\pi/2$. However, if $\kappa \neq 0$, θ will change along the fiber as dictated by Eq. (5), and energy will flow back into the two pumps in a periodic fashion. Thus, phase matching is critical for signal amplification and idler generation.

3 Single-Pump Parametric Amplifiers

In this section we focus on the degenerate FWM case in which a single intense pump is launched into a fiber together with the signal, and a single idler wave is generated through the degenerate FWM process. Equations (2)–(5) remain unchanged in the degenerate case provided we define ξ and κ as $\xi = \gamma P_1$ and $\kappa = \Delta\beta + 2\gamma P_1$. Integrating Eqs. (2) and (3) with the initial condition $B_4(0) = 0$, the signal power at the end of a fiber of length of L is found to be [1]

$$P_3(L) = P_3(0)\left[1 + (1 + \kappa^2/4g^2)\sinh^2(gL)\right], \tag{6}$$

where the parametric gain coefficient g and the phase mismatch κ are given by

$$g = \sqrt{(\gamma P_1)^2 - (\kappa/2)^2}, \qquad \kappa = \Delta\beta + 2\gamma P_1. \tag{7}$$

Equation (7) shows that the parametric gain is reduced by phase mismatch κ and is maximum when $\kappa = 0$. Both the nonlinear (SPM and XPM) and the linear effects (fiber dispersion) contribute to κ. Although the nonlinear contribution is constant at a given pump power, the linear phase mismatch depends on the wavelengths of the three waves. To realize net amplification of the signal, parametric gain g should be real. Thus, tolerable values of the linear phase mismatch $\Delta\beta$ are limited to the range $-4\gamma P_1 \leq \Delta\beta \leq 0$. The FOPA gain is maximum when the phase mismatch κ approaches zero, or when $\Delta\beta = -2\gamma P_1$. This relation indicates that optimal operation of FOPAs requires some amount of negative linear mismatch to compensate for the nonlinear phase mismatch. In fact, the bandwidth of the gain spectrum is determined by the pump power and the nonlinear parameter γ. Figure 1 shows this dependence clearly by plotting the parametric gain as a function of $\Delta\beta$ at three different power levels of a single pump [1].

The linear phase mismatch $\Delta\beta$ depends on the dispersion characteristics of the fiber. As the signal and idler frequencies are located symmetrically around the pump frequency ($\omega_4 = 2\omega_1 - \omega_3$), it is useful to

expand $\Delta\beta$ in a Taylor series around the pump frequency as [16]

$$\Delta\beta = \beta(\omega_3) + \beta(\omega_4) - 2\beta(\omega_1) = 2\sum_{m=1}^{\infty} \beta_{mp} \frac{(\omega_3 - \omega_1)^{2m}}{(2m)!}, \tag{8}$$

where $\beta_{mp} = (d^{2m}\beta/d\omega^{2m})_{\omega=\omega_1}$. This equation shows that only even-order dispersion parameters evaluated at the pump frequency contribute to the linear phase mismatch. Clearly, the choice of the pump wavelength is very critical while designing a FOPA. The linear phase mismatch $\Delta\beta$ is dominated by the second-order dispersion parameter β_{2p} when the signal wavelength is close to the pump but by the fourth- and higher-order dispersion parameters (β_{4p}, β_{6p}, etc.) when the signal deviates far from it. Thus, the ultimate FOPA bandwidth depends on the spectral range over which the linear phase mismatch is negative but large enough to balance the constant positive nonlinear phase mismatch of $2\gamma P_1$. This can be achieved by slightly displacing the pump wavelength from the ZDWL of the fiber such that β_{2p} is negative but β_{4p} is positive.

We should relate the parameters β_{2p} and β_{4p} to the fiber-dispersion parameters, $\beta_m = (d^m\beta/d\omega^m)_{\omega=\omega_0}$, calculated at the ZDWL of the fiber. This can be accomplished by expanding $\beta(\omega)$ in a Taylor series around ω_0. If we keep terms up to fourth-order in this expansion, we obtain

$$\beta_{2p} \approx \beta_3(\omega_1 - \omega_0) + \frac{\beta_4}{2}(\omega_1 - \omega_0)^2, \qquad \beta_{4p} \approx \beta_4. \tag{9}$$

Depending on the values of the fiber parameters β_3 and β_4, we can choose the pump frequency ω_1 such that β_{2p} and β_{4p} have opposite signs. More specifically, since both β_3 and β_4 are positive for most silica fibers, one should choose $\omega_1 < \omega_0$, i.e., the pump wavelength should be longer than the ZDWL of the fiber.

Figure 2 shows the gain spectra at several different pump wavelengths in the vicinity of the ZDWL λ_0 (chosen to be 1550 nm) by changing the pump detuning $\Delta\lambda_p = \lambda_1 - \lambda_0$ in the range -0.1 to $+0.15$ nm. The dotted curve shows the case $\Delta\lambda_p = 0$ for which pump wavelength coincides with the ZDWL exactly. The peak gain is about 8 dB and the gain bandwidth is limited to below 40 nm. When pump is tuned toward shorter-wavelength side, the bandwidth actually decreases. In contrast, both the peak gain and the bandwidth are enhanced by tuning the pump toward the longer-wavelength side. The signal gain in the vicinity of pump is the same regardless of pump wavelength. When signal wavelength moves away from the pump, the linear phase mismatch $\Delta\beta$ strongly depends on the pump wavelength. If both the third- and forth-order dispersion parameters are positive at ZDWL, according to Eq (9) the second order dispersion at the pump is negative when $\Delta\lambda_p$ is slightly positive, and thus can compensate for the nonlinear phase mismatch. This is the reason why gain peak is located at a wavelength far from the pump when $\lambda_1 > \lambda_0$. When phase matching is perfect ($\kappa = 0$), FOPA gain grows exponentially with the fiber length L as $G = 1 + \exp(2\gamma P_1 L)/4$. For the parameters used for Fig. 2, the best case occurs when $\Delta\lambda_p = 0.106$ nm. However, when $\Delta\lambda_p < 0$, both

the second- and forth-order dispersion parameters for the pump are positive. As a result, the linear phase mismatch adds up with with the nonlinear one, making κ relatively large. As a result, the FOPA bandwidth is reduced.

From a practical standpoint, one wants to maximize both the peak gain and the gain bandwidth at a given pump power P_1. Since peak gain is approximately given by $G_p \approx \exp(2\gamma P_1 L)/4$, its value increases exponentially as $\gamma P_1 L$, and can be increased by increasing fiber length. However, the gain bandwidth scales inversely with L because phase mismatch increases for longer fibers. The obvious solution is to use a fiber as short as possible. However, as the available amount of gain is a function of $\gamma P_1 L$, shortening of fiber length must be accompanied with an increase in the value of γP_1 to maintain the same amount of gain. This behavior is illustrated in Figure 3 where the gain bandwidth is shown to increase significantly when large value of γP_1 are combined with shorter lengths of fiber. The solid curve obtained for the 250-m-long fiber exhibits a 50-nm region on each side of the ZDWL over which the gain is nearly flat. Therefore, a simple rule of thumb for single-pump FOPAs is to use as high pump power as possible together with a fiber with as large a nonlinearity as possible. Since n_2 is fixed for silica fibers, the nonlinear parameter γ can be increased only by reducing the effective core area. Such fibers have become available in recent years and are called high-nonlinearity fibers (HNLFs) even though it is not the material nonlinearity n_2 that is enhanced in such fibers. Values of $\gamma > 10$ W^{-1}/km can be realized in such fibers. Photonic crystal fibers exhibiting high values of γ have also been used to build FOPAs [17]

HNLFs have been used to make FOPAs with a large bandwidth. In a 2001 experiment, a 200-nm gain bandwidth was realized by employing Raman-assisted parametric amplification inside a 20-m-long HNLF with $\gamma = 18$ W^{-1}/km [18]. The required pump power (~ 10 W) was large enough that signal was also amplified by stimulated Raman scattering when its wavelength exceeded the pump wavelength. Recent advances in designing microstructure fibers also make it possible to use short fiber lengths. A net peak gain of 24.5 dB over a bandwidth of 20 nm has been realized inside a 12.5-m-long microstructure fiber with $\gamma = 24$ W^{-1}/km pumped by high-energy pulses [17]. In another 2003 experiment, a peak gain of 43 dB with 85 nm bandwidth was obtained by pumping the FOPA with pulses at a repetition rate of 20 Gb/s [19]. However, a pulse-pumped FOPA requires either synchronization between the pump and signal pulses or pumping at a repetition rate much higher than that of the signal.

Another scheme for mitigating the phase-matching problem manages fiber dispersion along the fiber length, resulting in the so-called quasi-phase matching. This can be realized either through periodic dispersion compensation [20], [21] or by carefully arranging different sections of fiber with different dispersion properties [22]. As quasi-phase matching can be maintained along a fairly long length, continuous-wave

(CW) pumps can be used and still realize considerable amount of gain. Figure 4 shows the experimental results for such a single-pump FOPA [23] where both the net signal gain and the net conversion efficiency at the idler wavelength are shown at several pump-power levels. At a pump power of 31.8 dBm (about 1.5 W) at 1563 nm, the FOPA provided 49-dB peak gain. It was designed using a 500-m-long HNLF ($\gamma = 11$ W^{-1}/km) with low dispersion (dispersion slope $S = 0.03$ ps/nm^2/km). The fiber was composed of three sections with ZDWLs (1556.8, 1560.3, 1561.2 nm, respectively).

With its high gain over a wide spectrum, FOPAs have many practical applications. Simultaneous amplification of seven channels has been realized using a CW-pumped FOPA made of HNLF [24]. The experiment showed that dominant degradation stems from gain saturation and FWM-induced crosstalk among channels. FOPAs have also been used as a stable source of pulses at a high repetition rate (40 Gb/s) in long-haul transmission [25]. In another experiment, a transform-limited Gaussian-shape pulse train could be generated at a 40-Gb/s repetition when a weak CW signal was amplified using a FOPA whose pump power was sinusoidally modulated at 40 Gb/s [26].

As discussed earlier, all FOPAs generate the idler wave during signal amplification. Since the idler is a phase-conjugated version of the signal, it carries all the information associated with a signal and thus can be used for wavelength conversion. Indeed, FOPAs can act as highly efficient wavelength converters with a wide bandwidth [3]. As early as 1998, peak conversion efficiency of 28 dB was realized over 40-nm bandwidth (full width of the gain spectrum) using a pulsed pump [27]. More recently, transparent wavelength conversion (conversion efficiency > 0 dB) over 24-nm bandwidth (entire pump tuning range) was realized using a single-pump FOPA made with just 115 m of HNLF [28]. The ultrafast nature of nonlinear response of FOPAs is also useful for many other applications such as optical time-division demultiplexing [29] and optical sampling [30]. FOPAs can be used to mitigate noise associated with an input signal when operating in the saturation regime [31]. A similar scheme can be used for all-optical signal regeneration using a higher-order idler [32], [33]. FOPAs can also work in the pump-depleted region and can transfer as much as 92% of the pump power to the signal and idler fields [34]. Such FOPAs can be used to realize CW-pumped optical parametric oscillators with 30% internal conversion efficiency and a tuning range of 80 nm [35].

The performance of single-pump FOPAs is affected by several factors that must be considered during the design of such devices. For example, although FOPAs benefit from an ultrafast nonlinear response of silica, they also suffer from it because any fluctuations in the pump power are transferred to the signal and idler fields. As a result, noise in FOPAs is dominated by transfer of relative intensity noise (RIN) associated with the pump laser [3], [36]-[38]. Moreover, since the pump beam is typically amplified using one or two erbium-doped fiber amplifiers (EDFAs) to achieve high powers necessary for pumping an FOPA, amplified

spontaneous emission (ASE) from EDFAs can degrade the FOPA considerably. In fact, it is essential to block such ASE noise using optical filters. A noise figure of 4.2 dB with a maximum gain of 27.2 dB [39] and 3.7 dB with 17 dB gain [40] have been realized for parametric amplifiers. Similarly, a noise figure of 3.8 dB with 40 dB conversion efficiency has been reported for FOPA-based wavelength converters [41] by blocking the ASE noise through narrow-band fiber Bragg gratings. Such values of noise figure are close to the fundamental quantum limit of 3 dB [42].

The second factor that affects FOPAs is the nonlinear phenomenon of stimulated Brillouin scattering (SBS). The SBS threshold is around 10 mW for long fibers (>10 km) and increases to ∼0.1 W for fiber lengths of 1 km or so [1]. Since FOPAs require pump-power levels approaching 1 W, a suitable technique is needed that raises the threshold of SBS and suppresses it over the FOPA length. The techniques used in practice include control of temperature distribution along the fiber length [28] and phase modulation of the pump either at several fixed frequencies [23] or over a broad frequency range (using a pseudo-random bit pattern) [41]. The later technique suppresses SBS by broadening the pump spectrum. Although the amplified signal is affected little by spectral broadening of pump, unless group-velocity mismatch between pump and signal is relatively large [43], idler is affected much more drastically. In fact, the spectrum of idler can become twice as broad as the pump if the signal spectrum is narrow. This follows directly from the energy conservation or Eq. (1). The broadening of idler is not of concern when FOPAs are used for signal amplification but becomes a serious issue when they are used as wavelength converters. This problem can be solved by modulating the phases of the signal or the pumps synchronously. These techniques will be discussed in the following section.

The third issue associated with the single-pump FOPA is that its gain spectrum is not as uniform as one would like. In practice, only the pump wavelength can be adjusted to optimize the gain spectrum. As discussed before, the phase mismatch κ should be zero at the gain peak. However, Eq. (8) shows that it is hard to maintain this phase-matching condition over a wide bandwidth in a single-pump FOPA. Since $\Delta\beta \to 0$ when the signal wavelength approaches the pump wavelength, $\kappa \to 2\gamma P_1$. This value of κ is quite large and results in only a linear growth of gain ($G = 1 + \gamma P_1 L$). The net result is that the signal gain is considerably reduced in the vicinity of the pump wavelength, and the gain spectrum exhibits a dip. Figure 5 shows how variations in the phase mismatch κ affect the FOPA gain. Although κ can be close to zero in the spectral region where the FOPA gain peaks, it changes over a large range within the whole gain spectrum. The nonuniform gain of single-pump FOPAs is a consequence of such κ variations. Although amplification over a range as wide as 200 nm is possible, the gain spectrum remains highly nonuniform [18]. In practice, the usable bandwidth is limited to a much smaller region of the whole gain bandwidth. This problem can

be solved to some extent by manipulating fiber dispersion [20]–[22]. It is predicted theoretically that a fairly flat gain spectrum is possible by using several fiber sections of suitable lengths and properly selecting dispersive properties of these fiber sections [44], [45]. However, such a scheme is difficult to implement in practice because dispersive properties of HNLFs are rarely known with sufficient precision. The current practical solution is to make use of dual-pumped FOPAs discussed in the next section.

The fourth serious issue is the polarization dependence of the FOPA gain. The theoretical analysis in this section is based on the assumption that all optical fields are linearly polarized initially and maintain their state of polarization (SOP) during propagation inside the fiber. In practice, the SOP of the input signal can be arbitrary. The FWM process is highly polarization dependent because it requires angular momentum conservation among the four interacting photons [46]. Polarization-independent operation of single-pump FOPAs can be realized by employing a polarization-diversity loop [47], [48]. In this approach, the pump beam is split into its orthogonally polarized components with equal amount of powers, which counterpropagate inside a Sagnac loop. When the signal enter the loop, it is also split into its orthogonally polarized components, each of which copropagates with the identically polarized pump. The two polarization components of the signal are then recombined after the polarization-diversity loop. Such polarization-diversity loops have been used for optical sampling at 80 Gb/s with a residual polarization dependence of only 0.7 dB [49]. By using a polarization-maintaining HNLF inside such a loop, the wavelengths of 32 channels, each operating at 10 Gb/s, were converted simultaneously with a polarization dependence of only 0.2 dB [50].

4 Dual-Pump Parametric Amplifiers

Dual-pump FOPAs employ the nondegenerate FWM process using two pumps with different frequencies [51]. The properties of such FOPAs have been analyzed in recent years [4]–[6]. The most interesting aspect is that they can provide relatively flat gain over a much wider bandwidth than that possible for single-pump FOPAs. In the case of nondegenerate FWM, two distinct photon, one from each pump, are used to create the signal and idler photons as shown in Eq. (1). The parametric gain coefficient in this case can be obtained from the simple theory of Section 2 and is found to be [1]

$$g = \sqrt{(2\gamma)^2 P_1 P_2 - (\kappa/2)^2}, \tag{10}$$

where the phase mismatch $\kappa = \Delta\beta + \gamma(P_1 + P_2)$ and P_1 and P_2 are the input pump powers, assumed to remain undepleted.

Similar to the single-pump case, one can expand the linear phase mismatch $\Delta\beta = \beta(\omega_3) + \beta(\omega_4) - \beta(\omega_1) - \beta(\omega_2)$ in a Taylor series. A simple solution is to introduce $\omega_c = (\omega_1 + \omega_2)/2$ as the mean frequency

of the two pumps and $\omega_d = (\omega_1 - \omega_2)/2$ as the half of their frequency difference, and expand $\Delta\beta$ around ω_c [52]:

$$\Delta\beta = 2\sum_{m=1}^{\infty} \frac{1}{(2m)!}\left(\frac{d^{2m}\beta}{d\omega^{2m}}\right)_{\omega=\omega_c} \left[(\omega_3 - \omega_c)^{2m} - \omega_d^{2m}\right]. \tag{11}$$

This equation differs from Eq. (8) by the last term. This ω_d term contributes only when two pumps are used and is independent of the signal and idler frequencies. This difference provides the main advantage of dual-pump FOPAs over single-pump FOPAs as the ω_d term can be used to control the phase mismatch. By properly choosing the pump wavelengths, it is possible to use this term for compensating the nonlinear phase mismatch $\gamma(P_1 + P_2)$ stemming from SPM and XPM. As a result, the total phase mismatch κ can be maintained close to zero over a quite wide spectral range after the first term is made small by balancing carefully different orders of fiber dispersion.

The most commonly used configuration of dual-pump FOPAs employs a relatively large wavelength difference between the two pumps for realizing flat gain over a wide spectral range. This increases the magnitude of the ω_d term so that linear phase mismatch is large enough to compensate for nonlinear phase mismatch. At the same time, the mean frequency of the two pumps ω_c is set close to the ZDWL of the fiber so that the linear phase mismatch in Eq. (11) is kept constant over a broad range of ω_3. Therefore, to achieve a fairly wide phase matching range, the two pump wavelengths should be located on the opposite sides of the ZDWL in a symmetric fashion, but should be reasonably far from it [4]. Figure 5 shows how κ can be reduced to zero over a wide wavelength range using such a scheme, resulting in a flat broadband gain spectrum. Comparing the single-pump and dual-pump cases, it can be seen that although single-pump FOPAs may provide nonuniform gain over a wider bandwidth under certain conditions, the dual-pump FOPA provide much more uniform in general.

The preceding discussion is based on the assumption that only the nondegenerate FWM process contributes to FOPA gain. However, the situation is much more complicated for dual-pump FOPAs because the degenerate FWM process associated with each intense pump always occurs simultaneously with the nondegenerate one. In fact, it turns out that the combination of degenerate and nondegenerate FWM processes can create eight other idler fields besides the one at the frequency ω_4 [2]. Only four among these idlers, say at frequencies ω_5, ω_6, ω_7, and ω_8, are significantly relevant for describing the gain spectrum of FOPA because they are related to the signal frequency through the relations:

$$2\omega_1 \rightarrow \omega_3 + \omega_5, \qquad 2\omega_2 \rightarrow \omega_3 + \omega_6, \tag{12}$$

$$\omega_1 + \omega_3 \rightarrow \omega_2 + \omega_7, \qquad \omega_2 + \omega_3 \rightarrow \omega_1 + \omega_8. \tag{13}$$

Although these degenerate and nondegenerate FWM processes look as simple as Eq. (1) at the first glance, they do not occur independently because energy conversion is also maintained among the following processes:

$$2\omega_1 \rightarrow \omega_4 + \omega_7, \qquad 2\omega_2 \rightarrow \omega_4 + \omega_8, \tag{14}$$

$$\omega_1 + \omega_2 \rightarrow \omega_5 + \omega_8, \qquad \omega_1 + \omega_2 \rightarrow \omega_6 + \omega_7, \tag{15}$$

$$\omega_1 + \omega_4 \rightarrow \omega_2 + \omega_5, \qquad \omega_1 + \omega_6 \rightarrow \omega_2 + \omega_4. \tag{16}$$

All of these processes involve at least two photons from one or both intense pumps and will occur in the same order as the process in Eq (1) as long as their phase matching conditions are satisfied. As a result, a complete description of the FWM processes inside dual-pump FOPA becomes quite complicated [4]. Fortunately, a detailed analysis shows that the phase matching conditions associated with these processes are quite different. When the two pumps are located symmetrically far from the ZDWL of the fiber, the ten FWM processes shown in Eqs. (12)–(16) can only occur when the signal is in the vicinity of the two pumps. Thus, they leave unaffected the central flat part of the parametric gain spectrum resulting from the the process shown in Eq. (1), which is mainly used in practice. Figure 6 compares the FOPA gain spectrum obtained numerically using a complete analysis that includes all five idlers model (Solid curve) with that obtained using the sole nondegenerate FWM process of Eq. (1). It can be seen clearly that the flat portion of the gain spectrum has its origin in the single FWM process of Eq. (1). Other 10 processes only affect the edges of gain spectrum and reduce the gain bandwidth by 10–20%. We thus conclude that a model based on Eq. (1) is sufficient to describe the performance of dual-pump FOPAs as long as the central flat gain region is used experimentally.

Dual-pump FOPAs provide several degrees of freedom to realize a flat gain spectrum using just a single piece of fiber. By symmetrically assigning the two pumps on the opposite side of the ZDWL, a flat spectrum with high gain value has been obtained [53]. Since the two pumps are at the edge of the gain spectrum, pump blocking is no longer necessary, unlike the case of single-pump FOPAs. Moreover, as the pump power is distributed over two lasers in a dual pump FOPA, the required launched power for each pump laser is only half of that of the single-pump case. Figure 7 shows the data obtained in a recent experiment [54]. By using two pumps with powers of 600 mW at 1559 nm and 200 mW at 1610 nm, a gain of more than 40-dB over a 33.8-nm bandwidth was obtained inside a 1-km-long HNLF for which $\gamma = 17$ W^{-1}/km, ZDWL = 1583.5 nm, $\beta_3 = 0.055$ ps^3/km and $\beta_4 = 2.35 \times 10^{-4}$ ps^4/km. The solid curve shows the theoretical prediction.

Although phase modulation of the pumps is still necessary to suppress SBS, spectral broadening of the

idler is no longer a problem when the phases of signal or two pumps can be manipulated such that a specific idler is not broadened, depending on which idler is used for wavelength conversion. If ω_4 in Eq. (1) is used for wavelength conversion, the two pumps should be modulated out of phase [55] or using binary phase shift keying two pump phases can be altered in phase by π [56]. However, if ω_7 or ω_8 in Eq. (13) is used, the two pumps should be modulated in phase [57]. In the case of single pump FOPA, idler spectrum broadening can also be eliminated by modulating the signal phase at a rate twice of that used for modulating the pump phase [58], [59]. When counterphase modulation is used, higher-order idler generation in a dual-pump FOPA is shown to provide optical regeneration with a high extinction ratio and without spectral broadening [60].

Similar to the single-pump case, the gain in Dual-pump FOPAs is also strongly polarization dependent if no precaution is taken to mitigate the polarization effects [6], [46], [61]. Apart from the polarization-diversity loop used for single-pump FOPAs, polarization independent operation of a dual-pump FOPA can also be realized by using orthogonally polarized pumps [46], [56], [62]-[65]. When the two pumps are linearly but orthogonally polarized, the nondegenerate FWM process becomes completely polarization independent. In one experiment, a small polarization-dependent gain (PDG) of only 1 dB was observed when the signal was amplified by 15 dB over 20-nm bandwidth [65].

A practical issue associated with dual-pump FOPA is the Raman-induced power transfer between the two pumps. As shown in Eq. (4), the FWM efficiency ξ is proportional to $\sqrt{P_1 P_2}$ for a nondegenerate process and is maximized when the two pump powers are the same ($P_1 = P_2$). However, as the two pumps are far from each other but still within the bandwidth of the Raman-gain spectrum, stimulated Raman scattering can transfer energy from the pump of high frequency to that of low frequency. Since the two pumps cannot maintain equality in their powers along the fiber, a significant reduction occurs in the FWM efficiency even though the total power of the two pumps remains constant. To reduce this effect, the power of high-frequency pump is chosen to be higher than that of the low-frequency pump at the input end of the fiber. With this scheme, the two pump can maintain their powers close to each other over most of the fiber. Although Raman-induced pump power transfer reduces the FOPA gain by a considerable amount, it does not affect the shape of the gain spectrum since phase matching depends on the total power of the two pumps which is conserved inside FOPA as long as the two pumps are not depleted too much.

5 Fluctuations of Zero-Dispersion Wavelength

In the preceding sections, the fiber used to make an FOPA was assumed to be free from any fluctuations in its material properties. However, it is difficult to realize such ideal conditions. In practice, optical waves

in a realistic fiber undergo random perturbations originating from imperfections in the fiber. Two such imperfections are related to random variations along the fiber length in the ZDWL and residual birefringence, both of which originate partly from random changes in the core shape and size. In this section, we focus on ZDWL variations and consider the effects of residual birefringence in the next section. As dual-pump FOPAs provide much flatter gain spectra and are more likely to be used for telecommunication applications, we consider such FOPAs but limit our attention to the sole nondegenerate FWM process given in Eq. (1). As pointed out in the last section, this process is sufficient to describe the main flat portion of FOPA gain as long as the two pumps are located far from each other.

As seen clearly in Fig. 2, FOPA gain spectrum is extremely sensitive to dispersion parameters of the fiber. Changes in the ZDWL by as small as 0.05 nm change the gain spectrum considerably. Broad and flat gain spectra for dual-pump FOPAs were obtained in Section 4 by assuming that the dispersion characteristics of the fiber do not change along the fiber. However, this is not the case in reality. Fluctuations in the core shape and size along the fiber length make the ZDWL of the fiber to change randomly. As such perturbations typically occur during the drawing process, they are expected to have a small correlation length ($\sim$ 1 m). Long-term variations may also cause the ZDWL to vary over length scales comparable to fiber lengths used for FOPAs [66]. In general, ZDWL fluctuates only by a few nanometers, and the standard deviation of such fluctuations is a small fraction ($<$0.1%) of the mean ZDWL of the fiber.

In the presence of random ZDWL variations along the fiber, the growth of signal and idler waves is still governed by Eqs. (2) and (3) but the linear phase mismatch $\Delta\beta$ becomes a random function of z. As discussed before, considerable amount of linear phase mismatch should be maintained over the main portion of the bandwidth to optimize and flatten the FOPA gain spectrum. Since the contribution of ZDWL fluctuations $\delta\lambda_0$ is much smaller than the average value of linear phase mismatch, we can expand $\Delta\beta$ in a Taylor series to the first order as

$$\Delta\beta \approx K_1 + K_2\delta\lambda_0, \tag{17}$$

where $K_1 = \langle\Delta\beta\rangle$ is the average value and K_2 can be obtained from Eq. (8) or (11). The random variable $\delta\lambda_0$ can be modelled as a Gaussian stochastic process. If the correlation length l_c of ZDWL fluctuations is much smaller than the fiber length used for FOPA, the first order and second order moments of $\delta\lambda_0$ are given by

$$\langle\delta\lambda_0\rangle = 0, \qquad \langle\delta\lambda_0(z)\delta\lambda_0(z')\rangle = D_\lambda^2\,\delta(z-z'), \tag{18}$$

where the diffusion coefficient D_λ is related to the standard deviation σ_λ of ZDWL fluctuations and their correlation length l_c as $D_\lambda^2 = \sigma_\lambda^2 l_c$.

The main question is how the gain spectrum is affected by ZDWL fluctuations. It turns out that the

average value of signal or idler power can be found analytically [67]. After averaging Eqs. (2) and (3) over random ZDWL fluctuations [68], the evolution of the average signal/idler power is governed by the following three equations:

$$\frac{d\langle S_0\rangle}{dz} = -2\xi\langle S_3\rangle, \tag{19}$$

$$\frac{d\langle S_2\rangle}{dz} = -\frac{1}{2}D_\lambda^2 K_2^2\langle S_2\rangle + \kappa_a\langle S_3\rangle, \tag{20}$$

$$\frac{d\langle S_3\rangle}{dz} = -2\xi\langle S_0\rangle - \frac{1}{2}D_\lambda^2 K_2^2\langle S_3\rangle - \kappa_a\langle S_2\rangle, \tag{21}$$

where $\kappa_a = K_1 + \gamma(P_1 + P_2)$ is the average phase-mismatch parameter, $S_0(z) = P_3(z) + P_4(z) = 2P_3(z) - P_3(0)$ represents the sum of signal and idler powers and the auxiliary variables S_2 and S_3 are introduced using $S_2 - iS_3 = 2B_3B_4$. By solving Eqs. (19)–(21), we obtain the average gain spectrum $G_{av} = \langle P_3(L)\rangle/P_3(0)$ under the impact of ZDWL fluctuations, and it can be written as

$$G_{av} = \frac{1}{2}\left[\sum_{i=1}^{3}\frac{(4g^2 + a_j a_k)e^{a_i L}}{(a_i - a_j)(a_i - a_k)} + 1\right], \tag{22}$$

where $i \neq j \neq k$ and a_i are the roots of the cubic polynomial $a^3 + 4(D_\lambda K_2)^2 a^2 + (4D_\lambda^4 K_2^4 + \kappa_a^2 - 4\xi^2)a - 8(D_\lambda K_2 \xi)^2$.

The solid curves in Fig. 8 shows the average gain spectrum obtained using Eq. (22) for a FOPA operating under the conditions of Fig. 6 using $\sigma_\lambda = 1$ nm and $l_c = 5$ and 50 m. The dashed curves show for comparison the results obtained numerically by solving the stochastic equations (2) and (3) and averaging over 100 random realizations. Clearly, the agreement is quite good. However, the analytical theory becomes less accurate for larger correlation lengths. All of these curves should be compared with the dotted flat curve obtained in the case of a constant value of ZDWL. Clearly, ZDWL fluctuations are detrimental for FOPAs as they affect mainly the flat portion of the gain spectrum. As discussed in the preceding section, the flat-gain region is obtained by carefully optimizing the linear phase mismatch $\Delta\beta$ so that it compensates the nonlinear part and results in the total phase mismatch $\kappa \approx 0$ over a fairly broad spectral range. Thus, it is not surprising that ZDWL fluctuations deteriorate mainly the flat portion of FOPA gain spectrum. Figure 8 shows that ZDWL variations of even ± 1 nm eliminate the flat portion of the gain spectrum and produce two narrow peaks in the vicinity of each pump wavelength because ZDWL fluctuations do not affect the gain around the two pumps. The analytical result agrees well with numerical simulation when the ZDWL correlation length is much shorter than the total fiber length but begins to deviate when the two are comparable. In the later case, analytical theory overestimates the degradation caused by random ZDWL variations.

The gain spectra shown in Fig. 8 do not show the spectrum expected for a specific FOPA but rather represent an ensemble average. In practice, the gain spectrum will vary over a wide range for an ensemble

of FOPAs that are otherwise identical. Figure 9(a) shows the individual gain spectra for 100 realizations obtained numerically by solving the stochastic equations (2) and (3). The parameters are identical to those used for the solid curves in Fig. 8 with $l_c = 5$ m that represents the average of these 100 spectra. It is evident that amplified signal can fluctuate over a wide range for different members of the ensemble even when $\sigma_\lambda = 1$ nm. The important question is how one can design FOPAs that can tolerate ZDWL variations $\sim$1 nm? The answer turns out to be that the wavelength separation between the two pumps should be reduced significantly so that the second term in Eq. (11) does not play a major role. Of course, the whole gain spectrum is then much narrower, and the FOPA bandwidth is significantly reduced. However, this reduced-bandwidth gain spectrum is much more tolerant of ZDWL fluctuations. This is evident in Fig. 9(b) obtained under conditions identical to those of Fig. 9(a) except that the two pump wavelengths are separated by 50 nm rather than 98 nm. The innermost curves in Fig. 8 shows the average spectrum in this case. Flatness of the average gain spectrum is nearly maintained under such conditions but the spectrum is much narrower.

Comparing Figs. 9(a) and 9(b) and their averages given in Fig. 8, it is clear that smaller the fluctuations in the gain spectra, the flatter is the average gain spectrum. In the presence of ZDWL fluctuations, gain is not changed close to pump wavelengths, and at the center of the spectrum gain can only be lower than the no-fluctuation case. As a result, if one can adjust the pump wavelengths so that the average gain spectrum given by Eq. (22) is flat and close to the maximum available gain, i.e, closer to the dotted curve in Fig. 8, the fluctuations in the gain spectra should be minimum. In order to quantify the flatness of the average gain spectrum we define a "degree of flatness" as $F = G_{min}/G_{max}$ where G_{min} and G_{max} are the minimum and the maximum values of the average gain between the two pump wavelengths. Figure 10 shows how the degree of flatness changes as a function of pump wavelength separation for several values of σ_λ. The parameters used for Fig 10 are the same as the ones used for Fig. 9(b). The main conclusion of is that by reducing the pump separation it is possible to make the gain spectrum insensitive to ZDWL fluctuations (at the expense of a narrow gain bandwidth). The larger the fluctuations the narrower must be the pump wavelength separation. We conclude this section by emphasizing that ZDWL fluctuations will limit in practice the usable bandwidth of a FOPA.

6 Effect of Residual Fiber Birefringence

Most fibers exhibit residual birefringence that fluctuates randomly along the fiber length. Such birefringence fluctuations induce polarization-mode dispersion (PMD) and randomize the SOP of any optical wave

propagating through the fiber [69, 70]. They change the relative orientation of the four waves, affect the angular-momentum conservation among the four photons during the FWM process, and thus seriously degrade the performance of FOPAs [6], [71], [72]. Because, the nonlinear processes contributing to parametric amplification depend on the SOPs of the fields, a vector theory of FWM is needed. In this section we present such a theory and discuss its impact on FOPA performance.

Adopting the Jones-vector notation for vector fields used in Ref. [69], the four equations governing the propagation of two pumps, signal and idler in presence of randomly fluctuating birefringence can be written as follows [73]

$$\frac{\partial|A_1\rangle}{\partial z} = (b_0\sigma_1+\beta_1)|A_1\rangle + \frac{i\gamma}{3}\Big(|A_1^*\rangle\langle A_1^*| + 2|A_2\rangle\langle A_2| + 2|A_2^*\rangle\langle A_2^*|\Big)|A_1\rangle, \tag{23}$$

$$\frac{\partial|A_2\rangle}{\partial z} = [b_0\sigma_1 + b_1(\omega_2-\omega_1)\sigma_1+\beta_2]|A_2\rangle + \frac{i\gamma}{3}\Big(|A_2^*\rangle\langle A_2^*| + 2|A_1\rangle\langle A_1| + 2|A_1^*\rangle\langle A_1^*|\Big)|A_2\rangle, \tag{24}$$

$$\begin{aligned}\frac{\partial|A_3\rangle}{\partial z} = {} & [b_0\sigma_1 + b_1(\omega_3-\omega_1)\sigma_1+\beta_3]|A_3\rangle + \frac{2i\gamma}{3}\Big[\sum_{j=1}^{2}\big(|A_j\rangle\langle A_j| + |A_j^*\rangle\langle A_j^*|\big)\Big]|A_3\rangle \\ & + \frac{2i\gamma}{3}\Big(|A_1\rangle\langle A_2^*| + |A_2\rangle\langle A_1^*| + \langle A_1^*|A_2\rangle\Big)|A_4^*\rangle,\end{aligned} \tag{25}$$

$$\begin{aligned}\frac{\partial|A_4\rangle}{\partial z} = {} & [b_0\sigma_1 + b_1(\omega_4-\omega_1)\sigma_1+\beta_4]|A_4\rangle + \frac{2i\gamma}{3}\Big[\sum_{j=1}^{2}\big(|A_j\rangle\langle A_j| + |A_j^*\rangle\langle A_j^*|\big)\Big]|A_4\rangle \\ & + \frac{2i\gamma}{3}\Big(|A_1\rangle\langle A_2^*| + |A_2\rangle\langle A_1^*| + \langle A_1^*|A_2\rangle\Big)|A_3^*\rangle,\end{aligned} \tag{26}$$

where $|A_j\rangle$ ($j = 1$ to 4) represents the Jones vector apart from a constant phase factor that depends on the total pump power and σ_1 is one of the 2×2 diagonal Pauli matrix with elements 1 and -1. The effects of residual birefringence are included through two random variables b_0 and b_1. They are defined using the Taylor expansion $b(\omega) \approx b_0 + b_1(\omega-\omega_1)$, where $b(\omega) = \omega\delta n(\omega)/c$ and $\delta n(\omega)$ denotes refractive-index fluctuations. The vector equations for the case of single pump can be deduced from these equations after minor modifications [74].

It is clear from Eqs. (23)–(26) that in the absence of b_1, all the fields will change their SOP in the same way. These equations are written using first pump as a reference. As a result, other three fields change their SOPs around the first pump at a rate given by the frequency difference $\omega_j - \omega_1$, where $j = 2,\ 3$, or 4. The random variable b_1 is also responsible for difference in the group velocity between pulses of different polarization and leads to PMD. In fact, the variance of b_1 is related to the PMD parameter D_p through the expression $\langle b_1^2\rangle = D_p^2/l_c$ [75], where l_c is the correlation length over which b_0 and b_1 change. Both b_0 and b_1 obey Gaussian statistics with zero mean.

Similar to the case of ZDWL fluctuations, one can use the stochastic equations (23)–(26) to calculate the average gain spectrum in the presence of PMD. In the case of single-pump FOPA, the average can be

performed analytically [74]. Figure 11 shows the analytic results (solid curves) and compares them with the direct numerical simulations (dashed curves) for $D_p = 0.05$ and 0.15 ps/$\sqrt{\text{km}}$. The dotted curve represents the expected gain in the absence of birefringence fluctuations. It is evident that random fluctuations of birefringence severely impact the FOPA gain spectrum. Random variables b_0 and b_1 affect the FOPA through two different mechanisms. While b_0 rotates the SOP of all four fields in the same manner and thus reduces the available average gain roughly by the same amount at all frequencies, b_1 causes pump and signal SOPs to drift from each other at a rate that depends on their frequency difference.

It is useful to define a diffusion length L_d as $L_d = 3/(D_p \Delta\omega)^2$; it quantifies the length scale over which two fields that has same SOPs initially develop random SOPs with respect to each other [76]. When L_d is much larger than the total fiber length, effects of b_1 are negligible. In a typical fiber, b_0 changes the SOP of fields over a length scale of 10 m. Because such changes take place over a much shorter scale than the nonlinear length and are same for all the fields, Eqs. (23)–(26) can be averaged over b_0. The main effect of b_0 is that the nonlinear parameter γ is reduced by a factor of 8/9. Since the efficiency of both FWM and XPM is reduced, the gain is lowered at the peaks from 28 to 24.5 dB but by only 1 dB in the central region. In Figure 11, the gain curve for $D_p = 0.05$ ps/$\sqrt{\text{km}}$ follows very closely this prediction. This is not surprising because $L_d = 2.1$ km for this low value of D_p is comparable to the total fiber length of 2 km even for as large as 30 nm separation between pump and signal. However, L_d is reduced to 0.24 km when $D_p = 0.15$ ps/$\sqrt{\text{km}}$, and the effects of b_1 takes over. As seen in Fig. 11, the gain is reduced by more than 10 dB and the spectrum is distorted considerably.

In the case of dual-pump FOPAs, the complexity of Eqs. (23-26) hinders an analytic treatment. For this reason, we solve these equations numerically for three different values of D_p. Figure 12 shows fluctuations in gain for $D_p = 0.1$ ps/$\sqrt{\text{km}}$ for 50 different realizations of random birefringence. Note that the birefringence parameters can change with time for a given fiber on a time scale ranging from seconds to hours. For this reason, gain fluctuations seen in Fig. 12 can also be viewed as fluctuations with time for a given FOPA. The average gain obtained from 50 realizations is shown in Figure 13 for three different values of D_p. The ideal case of isotropic fiber is also shown for comparison as a solid curve. Similar to the case of single-pump FOPA, the effect of b_0 is just to reduce the nonlinear coefficient γ by a factor 8/9 [75]. For the parameters used in Fig. 13, the lower value of γ reduces the peak gain from 37 to 33 dB but keeps the spectrum flat. The central dip seen in Fig. 13 results from b_1. The reason behind this dip can be understood as follows. When the signal frequency is close to one of the pumps, that pump provides the dominant contribution. However, as signal frequency moves towards the center of spectrum, neither of the two pumps remains oriented parallel to the signal, and the gain is reduced.

As discussed earlier, it is important that FOPAs provide gain that does not depend on the SOP of the input signal, and two methods are commonly used for this purpose. However, the random residual birefringence prevents these methods from working perfectly. The polarization-diversity method relies critically on the assumption that the signal and pump maintain their identical SOPs throughout the fiber. The second method utilizes orthogonal pumps and works only under the assumption that the pumps maintain their orthogonal SOPs throughout the fiber. It was already noted that fields with different frequencies change their SOP at different rates in the presence of PMD. It is thus evident that both of these schemes will introduce polarization-dependent gain (PDG). This was also observed experimentally when second method was implemented [72].

To illustrate the performance of the second method in the presence of PMD, we have performed numerical simulations using two pumps with linear but orthogonal SOPs initially. For each realization, signal is launched at an angle of $\theta = 0$, 45 and 90^0 from the pump at the shorter wavelength. Figure 14 shows the results for a PMD parameter $D_p = 0.1$ ps/$\sqrt{\text{km}}$. The expected gain curve in the absence of PMD is also shown as a dotted curve. For certain signal wavelengths, PDG can be as large as 12 dB, where PDG is defined as the difference between the maximum and minimum gain as the signal SOP is changed. PDG increases as the signal wavelength gets closer to either of the pumps. The same behavior was also observed in a 2003 experiment [72]. In physical terms, the reason why the largest PDG occurs for a signal close to pump wavelength can be understood as follows. If the signal has a wavelength close to one pump, their relative orientation does not change along the fiber but it decorrelates with the other pump rapidly because they are at the different edges of the spectrum. As a result, whatever the initial polarization of the second pump, the signal can only sense its average effect. However, because it keeps its relative orientation with the first pump, the signal experiences the highest or smallest gain depending on if it was initially parallel or orthogonal to the first pump. The reason why the overall gain is smallest in the case of isotropic fiber is that the FWM efficiency is the smallest when the pumps are orthogonal. PMD can make the pumps non-orthogonal (and even parallel occasionally) and hence, increases the gain.

7 Summary

In this review on FOPAs we have focused on some of the recent advances that have advanced considerably the state of the art for parametric amplifiers. The well-known simple theory behind the nonlinear phenomenon of FWM was discussed first to provide the background material. It was then used to discuss the performance of single-pump FOPAs and reveal the important role played by the nonlinear contribution to the

phase-matching condition. The same scalar theory was used to discuss the more general case of dual-pump FOPAs and show that the gain spectrum in such amplifiers results from several degenerate and nondegenerate FWM processes. However, it turns out that only a single nondegenerate process dominates in the case of FOPAs pumped at two wavelengths relatively far apart from each other and located on opposite sides of the ZDWL. We discuss the design of such FOPAs and show how they can be designed to provide a gain spectrum that is relatively uniform over a bandwidth larger than 100 nm.

The experiments on dual-pump FOPAs have shown that flat gain over a bandwidth of 40 nm or so can be realized in practice. To resolve this discrepancy between the theoretical and experimental results, we study impact of two unavoidable phenomena that affect the performance of all FOPA-based devices. First, the ZDWL of a fiber can vary along its length in a random fashion owing to core-diameter variations that occur invariably during fiber manufacturing. We show that ZDWL fluctuations as small as ± 1 nm degrade severely the gain spectrum of FOPAs because they mainly affect its central flat part. This degradation can be avoided to a large extent by moving pump wavelengths closer so that they are separated by about 40 to 50 nm instead of 100 nm or more. This appears to be the main reason why experiments have realized flat gain only over 40 nm or so. Second, birefringence fluctuations that occur in all practical fibers and lead to PMD also affect the gain spectrum of FOPAs. Their inclusion requires the development of a vector theory based on the Jones-matrix formalism that can also be related to the rotation of the SOP of each optical field on the Poincaré sphere. We discuss how PMD affects the gain spectrum and make the FOPA gain polarization dependent even when orthogonally polarized pumps are used.

Acknowledgements

This work is supported by the US National Science Foundation under grants ECS-0320816 and DMS-0073923.

References

[1] G. P. Agrawal, *Nonlinear Fiber Optics*, 3rd ed. (Academic Press, San Diego, 2001).

[2] J. Hansryd, P. A. Andrekson, M. Westlund, J. Li, and P. O. Hedekvist, "Fiber-based optical parametric amplifiers and their applications," IEEE J. Sel. Top. Quantum Electron. **8**, 506-520, (2002).

[3] M. N. Islam and Ö. Boyraz, "Fiber parametric amplifiers for wavelength band conversion," IEEE. J. Sel. Top. Quantum Electron. **8**, 527-537 (2002).

[4] C. J. McKinstrie, S. Radic and A. R. Chraplyvy, "Parametric amplifiers driven by two pump waves," IEEE J. Sel. Top. Quantum Electron. **8**, 538-547 (2002).

[5] S. Radic, C. J. McKinstrie, A. R. Chraplyvy, G. Raybon, J. C. Centanni, C. G. Jorgensen, K. Brar and C. Headley, "Continuous-wave parametric gain synthesis using nondegenerate pump four-wave mixing," IEEE Photon. Technol. Lett. **14**, 1406-1408 (2002).

[6] S. Radic and C. J. McKinstrie, "Two-pump fiber parametric amplifiers," Opt. Fiber. Technol. **9**, 7-23 (2003).

[7] A. Yariv, D. Fekete, and D. M. Pepper, "Compensation for channel dispersion by nonlinear optical phase conjugation," Opt. Lett. **4**, 52-54 (1979).

[8] S. Watanabe and M. Shirasaki, "Exact compensation for both chromatic dispersion and Kerr effect in a transmission fiber using optical phase conjugation," J. Lightwave Technol. **14**, 243-248 (1996).

[9] J. Santhanam and G. P. Agrawal, "Reduced timing jitter in dispersion-managed lightwave systems through parametric amplification," J. Opt. Soc. Am. B **20**, 284-291 (2003).

[10] C. J. McKinstrie, S. Radic, and C. Xie, "Reduction of soliton phase jitter by in-line phase conjugation," Opt. Lett. **28**, 1519-1561 (2003).

[11] J. A. Levenson, I. Abram, T. Rivera, and P. Grangier, "Reduction of quantum noise in optical parametric amplification," J. Opt. Soc. Am. B **10**, 2233-2238 (1993).

[12] I. H. Deutsch and I. Abram, "Reduction of quantum noise in soliton propagation by phase-sensitive amplification," J. Opt. Soc. Am. B **11**, 2303-2313 (1994).

[13] W. Imajuku, A. Takada, and Y. Yamabayashi, "Inline coherent optical amplifier with noise figure lower than 3 dB quantum limit," Electron. Lett. **36**, 63-64 (2000).

[14] R. W. Boyd, *Nonlinear Optics*, (Academic Press, San Diego, 1992).

[15] K. Inoue and T. Mukai, "Signal wavelength dependence of gain saturation in a fiber optical parametric amplifier," Opt. Lett. **26**, 10-12 (2001).

[16] M. E. Marhic, N. Kagi, T. K. Chiang, and L. G. Kazovsky, "Broadband fiber optical parametric amplifiers," Opt. Lett. **21**, 573-575 (1996).

[17] R. Tang, P. Devgan, J. Sharping, P. Voss, J. Lasri, P. Kumar, "Microstructure fiber based optical parametric amplifier in the 1550-nm Telecom band," Proc. Opt. Fiber Commun., (Optical Society of America, Washington, DC, 2003), pp. 562-563.

[18] M. Ho, K. Uesaka, M. Marhic, Y. Akasaka and L. G. Kazovsky, "200-nm-Bandwidth fiber optical amplifier combining parametric and Raman gain," J. Lightwave Technol. **19**, 977-981 (2001).

[19] K. Shimizu, K. Wong, G. Kalogerakis, K. Uesaka, M. Marhic, L. Kazovsky, "High repetition-rate pulsed-pump fiber OPA for 10Gb/s NPZ modulated signals," Proc. Opt. Fiber Commun., (Optical Society of America, Washington, DC, 2003), pp. 566-567.

[20] M. E. Marhic, F. S. Yang, M. Ho, L. G. Kazovsky, "High-nonlinearity fiber optical parametric amplifier with periodic dispersion compensation," J. Lightwave Technol. **17**, 210-215 (1999).

[21] J. Kim, Özdal Boyraz, J. H. Lim, and M. N. Islam, "Gain enhancement in cascaded fiber parametric amplifier with quasi-phase matching: Theory and experiment," J. Lightwave Technol. **19**, 247-251 (2001).

[22] K. Inoue, "Arrangement of fiber pieces for a wide wavelength conversion range by fiber four-wave mixing," Opt. Lett. **19**, 1189-1191 (1994).

[23] J. Hansryd and P. A. Andrekson, "Broad-band continuous-wave-pumped fiber optical parametric amplifier with 49-dB gain and wavelength-conversion efficiency," IEEE Photon. Technol. Lett. **13**, 194-196 (2001).

[24] T. Torounidis, H. Sunnerud, P. O. Hedekvist, and P. A. Andrekson, "Amplification of WDM signals in Fiber-Based optical parametric amplifiers," IEEE Photon. Technol. Lett. **15**, 1061-1063 (2003).

[25] T. Torounidis, H. Sunnerud, P. O. Hedekvist, and P. A. Andrekson, "40-Gb/s transmission using RZ-pulse source based on fiber optical parametric amplification," IEEE Photon. Technol. Lett. **15**, 1159-1161 (2003).

[26] J. Hansryd and P. A. Andrekson, "Wavelength tunable 40-GHz pulse source based on fiber optical parametric amplifier," Electron. Lett. **37**, 584-585 (2001).

[27] G. A. Nowak, Y. Hao, T. J. Xia, M. N. Islam and D. Nolan, "Low-power high-efficiency wavelength conversion based on modulational instability in high-nonlinearity fiber," Opt. Lett. **23**, 936-938 (1998).

[28] M. Westlund, J. Hansryd, P. A. Andrekson, and S. N. Knudsen, "Transparent wavelength conversion in fiber with 24 nm pump tuning range," Electon. Lett. **38**, 85-86 (2002).

[29] J. Hansryd and P. A. Andrekson, "O-TDM demultiplexer with 40-dB gain based on a fiber optical parametric amplifier," IEEE Photon. Technol. Lett. **13**, 732-734 (2001).

[30] J. Li, J. Hansryd, P. O. Hedekvist, P. A. Andrekson, and S. N. Knudsen, "300-Gb/s eye-diagram measurement by optical sampling using fiber-based parametric amplification," IEEE Photon. Technol. Lett. **13**, 987-989 (2001).

[31] Y. Su, L. Wang, A. Agarwal, and P. Kumar, "All-optical limiter using gain flattened fiber parametric amplifier," Electron. Lett. **36**, 1103-1104 (2000).

[32] E. Ciaramella and S. Trillo, "All-optical signal reshaping via four-wave mixing in optical fibers," IEEE Photon. Technol. Lett. **12**, 849-851 (2000).

[33] K. Inoue, "Suppression of level fluctuation without extinction ratio degradation based on output saturation in higher order optical parametric interaction in fiber," IEEE Photon. Technol. Lett. **13**, 338-340 (2001).

[34] M. E. Marhic, K. K. Y. Wong, M. C. Ho, and L. G. Kazovsky, "92% pump depletion in a continuous-wave one-pump fiber optical parametric amplifier," Opt. Lett. **26**, 620-622 (2001).

[35] M. E. Marhic, K. K. Y. Wong, L. G. Kazovsky, and T. E. Tsai, "Continuous-wave fiber optical parametric oscillator," Opt. Lett. **27**, 1439-1441 (2002).

[36] X. Zhang and B. F. Jorgensen, "Noise characteristics and optimization fiber length of spectral inversion using four-wave mixing in a dispersion-shifted fiber," Opt. Fiber Technol. **3**, 28-43 (1997).

[37] P. O. Hedekvist and P. A. Andrekson, "Noise characteristics of fiber-based optical phase conjugators," J. Lightwave Technol. **17**, 74-79 (1999).

[38] P. Kylemark, P. O. Hedekvist, H. Sunnerud, and M. Karlsson, P. A. Andrekson, "Noise characteristics of fiber optical parametric amplifiers," J. Lightwave Technol. **22**, 409-416 (2004).

[39] J. L. Blows and S. E. French, "Low-noise-figure optical parametric amplifier with a continuous-wave frequency-modulated pump," Opt. Lett. **27**, 491-493 (2002).

[40] P. L. Voss, R. Tang, and P. Kumar, "Measurement of the photon statistics and the noise figure of a fiber-optic parametric amplifier," Opt. Lett. **28**, 549-551 (2003),

[41] K. K. Y. Wong, K. Shimizu, M. E. Marhic, K. Uesaka, G. Kalogerakis, and L. G. Kazovsky, "Continuous-wave fiber optical parametric wavelength converter with 40 dB conversion efficieny and a 3.8 dB noise figure," Opt. Lett. **28**, 692-694 (2003).

[42] G. P. Agrawal, *Fiber-Optic Communication Systems*, 3rd ed. (Wiley, New York, 2002).

[43] A. Mussot, A. Durecu-Legrand, E. Lantz, C. Simonneau, and D. Bayart, "Impact of pump phase modulation on the gain of fiber optical parametric amplifier," IEEE Photon. Technol. Lett. **16**, 1289-1291 (2004).

[44] L. Provino, A. Mussot, E. Lantz, T. Sylvestre, and H. Maillotte, "Broadband and flat parametric amplifiers with a multisection dispersion-tailored nonlinear fiber arrangement," J. Opt. Soc. Am. B **20**, 1532-1537 (2003).

[45] W. Zhang, C. Wang, J. Shu, and W. Hu, "Design of fiber-optical parametric amplifiers by genetic algorithm," IEEE Photon. Technol. Lett. **16**, 1652-1654 (2004).

[46] Q. Lin and G. P. Agrawal, "Vector theory of four-wave mixing: polarization effects in fiber-optic parametric amplifiers," J. Opt. Soc. Am. B **21**, 1216-1224 (2004).

[47] T. Hasegawa, K. Inoue, and K. Oda, "Polarization independent frequency conversion by fiber four-wave mixing with a polarization diversity technique," IEEE Photon. Technol. Lett. **5**, 947-949 (1993).

[48] K. K. Y. Wong, M. E. Marhic, K. Uesaka, and L. G. Kazovsky, "Polarization-independent one-pump fiber-optical parametric amplifier," IEEE Photon. Technol. Lett. **14**, 1506-1508 (2002).

[49] A. Tersigni, V. Calle, A. T. Clausen, L. K. Oxenłłwe, J. Młrk and P. Jeppesen, "Polarization independent optical sampling using four-wave mixing," Conf. Lasers & Electro-Optics, (Optical Society of America, Washington, DC, 2003), paper CMR2.

[50] S. Watanabe, S. Takeda, and T. Chikama, "Interband wavelength conversion of 320 Gb/s (32×10Gb/s) WDM signal using a polarization-insensitive four-wave mixer," ECOC98, p85-86 (1998).

[51] C. J. McKinstrie and S. Radic, "Parametric amplifiers driven by two pump waves with dissimilar frequencies," Opt. Lett. **27**, 1138-1140 (2002).

[52] M. E. Marhic, Y. Park, F. S. Yang, and L. G. Kazovsky, "Broadband fiber-optical parametric amplifiers and wavelength converters with low-ripple Chebyshev gain spectra," Opt. Lett. **21**, 1354-1356 (1996).

[53] S. Radic, C. J. McKinstrie, A. R. Chraplyvy, G. Raybon, J. C. Centanni, C. G. Jorgensen, K. Brar, and C. Headley, "Continuous-wave parametric gain synthesis using nondegenerate pump four-wave mixing," IEEE Photon. Technol. Lett. **14**, 1406-1408 (2002).

[54] S. Radic, C. J. McKinstrie, R. M. Jopson, J. C. Centanni, Q. Lin and G. P. Agrawal, "Record performance of parametric amplifier constructed with highly nonlinear fibre," Electron. Lett. **39**, 838-839 (2003)

[55] M. Ho, M. E. Marhic, K. Y. K. Wong, and L. G. Kazovsky, "Narrow-linewidth idler generation in fiber four-wave mixing and parametric amplification by dithering two pumps in opposition of phase," J. Lightwave Technol. **20**, 469-476 (2002).

[56] T. Tanemura and K. Kikuchi, "Polarization-independent broad-band wavelength conversion using two-pump fiber optical parametric amplification without idler spectral broadening," IEEE Photon. Technol. Lett. **15**, 1573-1575 (2003).

[57] S. Radic, C. J. McKinstrie, R. M. Jopson, J. C. Centanni, A. R. Chraplyvy, C. G. Jorgensen, K. Brar, and C. Headley, "Selective suppression of idler spectral broadening in two-pump parametric architectures," IEEE Photon. Technol. Lett. **15**, 673-675 (2003).

[58] K. Torii and S. Yamashita, "Cancellation of spectral spread by pump frequency modulation in optical fiber wavelength converter," OFC01, WW5-1 (2001).

[59] K. Torii and S. Yamashita, "Efficiency improvement of optical fiber wavelength converter without spectral spread using synchronous phase/frequency modulations," J. Lightwave Technol. **21**, 1039-1045 (2003).

[60] S. Radic, C. J. McKinstrie, R.M. Jopson, J. C. Centanni, and A. R. chrapyvy, "All-optical regeneration in one and two-pump parametric amplifier using highly nonlinear optical fiber," IEEE Photon. Technol. Lett. **15**, 957-959 (2003).

[61] A. Guimaraes, W. A. Arellano, M. O. Berendt, H. L. Fragnito, "Measurement of polarization dependent gain in a dual pump fiber optical parametric amplifier," Conf. Lasers & Electro-Optics, (Optical Society of America, Washington, DC, 2001), pp. 447-448.

[62] R. M. Jopson and R. E. Tench, "Polarization-independent phase conjugation of lightwave signals," Electron. Lett. **29**, 2216-2217 (1993).

[63] K. Inoue, "Polarization independent wavelength conversion using fiber four-wave mixing with two orthogonal pump lights of different frequencies," J. Lightwave Technol. **12**, 1916-1920 (1994).

[64] S. Yamashita and K. Torii, "Polarization-independent highly-efficient optical fiber wavelength converter," Conf. Lasers & Electro-Optics, (Optical Society of America, Washington, DC, 2001), pp. 384-385.

[65] K. K. Y. Wong, M. E. Marhic, K. Uesaka, and L. G. Kazovsky, "Polarization-independent two-pump fiber optical parametric amplifier." IEEE Photon. Technol. Lett. **14**, 911-913 (2002).

[66] M. Karlsson, "Four-wave mixing in fibers with randomly varying zero-dispersion wavelength," J. Opt. Soc. Am. B **15**, 2269-2275 (1998).

[67] F. Yaman, Q. Lin, S. Radic, and G. P. Agrawal, "Impact of dispersion fluctuations on dual-pump fiber-optic parametric amplifiers," IEEE Photon Technol. Lett. **16**, 1292-1294 (2004).

[68] C. W. Gardiner, *Handbook of Stochastic Methods*, 2nd ed. (Springer, New York, 1985).

[69] J. P. Gordon and H. Kogelnik, "PMD fundamentals: Polarization mode dispersion in optical fibers," Proc. Natl. Acad. Sci. USA **97**, 4541-4550 (2000).

[70] H. Kogelnik, R. M. Jopson, and L. E. Nelson, "Polarization-Mode Dispersion," in *Optical Fiber Telecommunications IV B*, I. P. Kaminow and T. Li, Eds. (Academic, San Diego, 2002), Chap. 15.

[71] P. O. Hedekvist, M. Karlsson, and P. A. Andrekson, "Polarization dependence and efficiency in a fiber four-wave mixing phase conjugator with orthogonal pump waves," IEEE Photon Technol. Lett. **8**, 776-778 (1996).

[72] S. Radic, C. McKinstrie, R. Jopson, C. Jorgensen, K. Brar, and C. Headley, "Polarization dependent parametric gain in amplifiers with orthogonally multiplexed optical pumps," OFC03, p508-509 (2003).

[73] F. Yaman, Q. Lin, G. P. Agrawal, "Effects of polarization-mode dispersion in dual-pump fiber-optic parametric amplifiers," IEEE Photon Technol. Lett. **16**, 431-433 (2004).

[74] Q. Lin, G. P. Agrawal, "Effects of polarization-mode dispersion on fiber-based parametric amplifiers and wavelength conversion," Opt. Lett., **29**, 1114-1116, (2004).

[75] P. K. A. Wai and C. R. Menyuk, "Polarization mode dispersion, decorrelation, and diffusion in optical fibers with randomly varying irefringence," J. Lightwave Technol. **14**, 148-157 (1996).

[76] M. Karlsson and J. Brentel, "Autocorrelation function of the polarization-mode dispersion vector," Opt. Lett. **24**, 939-941, (1999).

Figure Captions

1. Parametric gain for a single-pump FOPA as a function of linear phase mismatch at three pump powers P_0 for a fiber with $\gamma = 10$ W^{-1}/km.

2. Gain spectra for a single-pump FOPA for several values of pump detuning $\Delta\lambda_p = \lambda_p - \lambda_0$ from the ZDWL λ_0. The parameters used are $\gamma = 2$ W^{-1}/km, $P_1 = 0.5$ W, $L = 2.5$ km, $\beta_3 = 0.1$ ps^3/km, and $\beta_4 = 10^{-4}$ ps^4/km.

3. Gain spectra for single-pump FOPAs of three different lengths. The product $\gamma P_1 L = 6$ is kept constant for all curves. Other parameters are the same as those used for Figure 2.

4. (a) Measured signal gain and (b) idler conversion efficiency for a single-pump FOPA at several pump powers. Solid curves show the theoretically expected results. (Adapted from Ref. [23])

5. Optimized gain spectra for single-pump and dual-pump FOPAs and corresponding phase-mismatch κ. Same amount of total pump power was used in both cases.

6. Gain spectra for a dual-pump FOPA including the contribution of all idlers (solid curve). The dotted curve shows gain spectrum when only a single idler corresponding to the dominant nondegenerate FWM process is included. The parameters used are $L = 0.5$ km, $\gamma = 10$ W^{-1}/km, $P_1 = 0.5$ W, $P_2 = 0.5$ W, $\beta_3 = 0.1$ ps^3/km, $\beta_4 = 10^{-4}$ ps^4/km, $\lambda_1 = 1502.6$ nm, $\lambda_2 = 1600.6$ nm, and $\lambda_0 = 1550$ nm.

7. Measured (diamonds) and calculated (solid) gain spectrum as a function of signal wavelength for a dual-pump FOPA.

8. Average gain spectra for a dual-pump FOPA in which ZDWL varies randomly along the fiber with a standard deviation of 1 nm for $l_c = 5$ and 50 m. In each case, analytical and numerical results are compared. The thin solid curve shows the gain in the absence of fluctuations. The innermost curve shows the results for $l_c = 5$ m when pumps are spaced apart by only 50 nm. All other parameters are identical to those used for Fig. 6.

9. Changes expected in the gain spectra from fiber to fiber because of ZDWL fluctuations ($\sigma_\lambda = 1$ nm and $l_c = 5$ m) when pump spacing is 98 nm (top) or 50 nm (bottom). All other parameters are identical to those used for Fig. 6.

10. Degree of flatness plotted as a function of separation between pump wavelengths for several values of σ_λ.

11. Average gain spectrum for a single-pump FOPA for two values of the PMD parameter D_p. Solid and dashed curves compare the analytical and numerical results. Dotted curve shows the no-PMD case. Parameters values used are $\gamma = 2$ W^{-1}/km, $L = 2$ km, $\lambda_0 = 1550$ nm, $\beta_3 = 0.1$ ps^3/km, $\beta_4 = 10^-4$ ps^4/km, and $P_1 = 1$ W.

12. Changes in gain spectra with birefringence fluctuations for a dual-pump FOPA for $D_p = 0.1$ ps/$\sqrt{\text{km}}$. Other parameters are same as used in Fig. 6. Both pumps and the signal have the same SOP initially.

13. Average gain spectra for a dual-pump FOPA for three values of the PMD parameter with the same parameter values used in Fig. 6. Solid curve shows for comparison the no-PMD case.

14. Average gain versus signal wavelength for three different initial linear SOP of the signal when $D_p = 0.1$ ps/$\sqrt{\text{km}}$; θ represents the angle between the linear SOPs of signal and the shorter-wavelength pump. The other pump is orthogonally polarized. Dotted curve shows for comparison the no-PMD case.

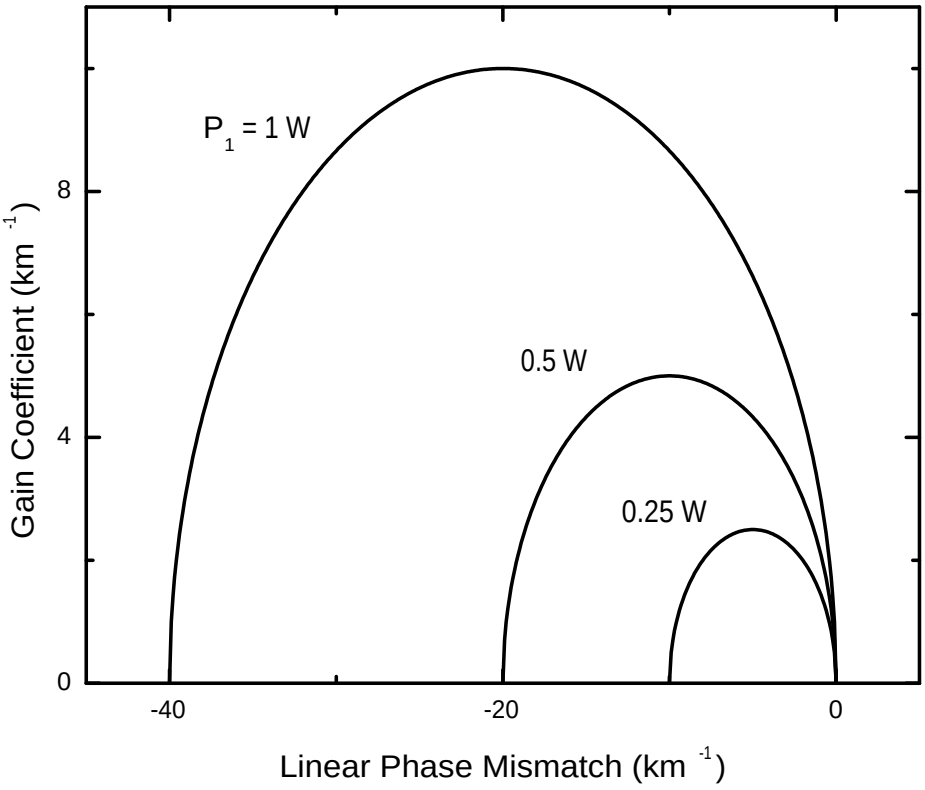

Figure 1 of Yaman et al.

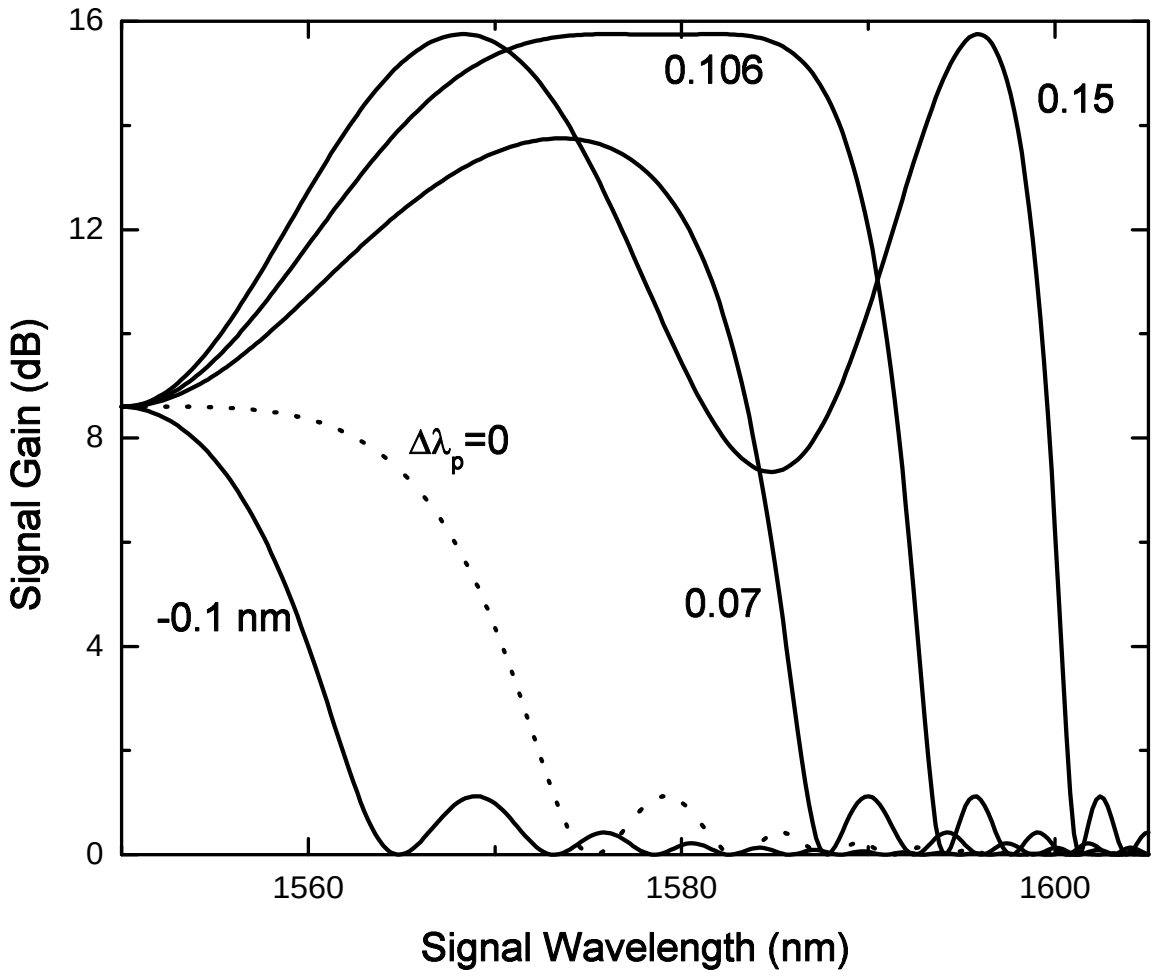

Figure 2 of Yaman et al.

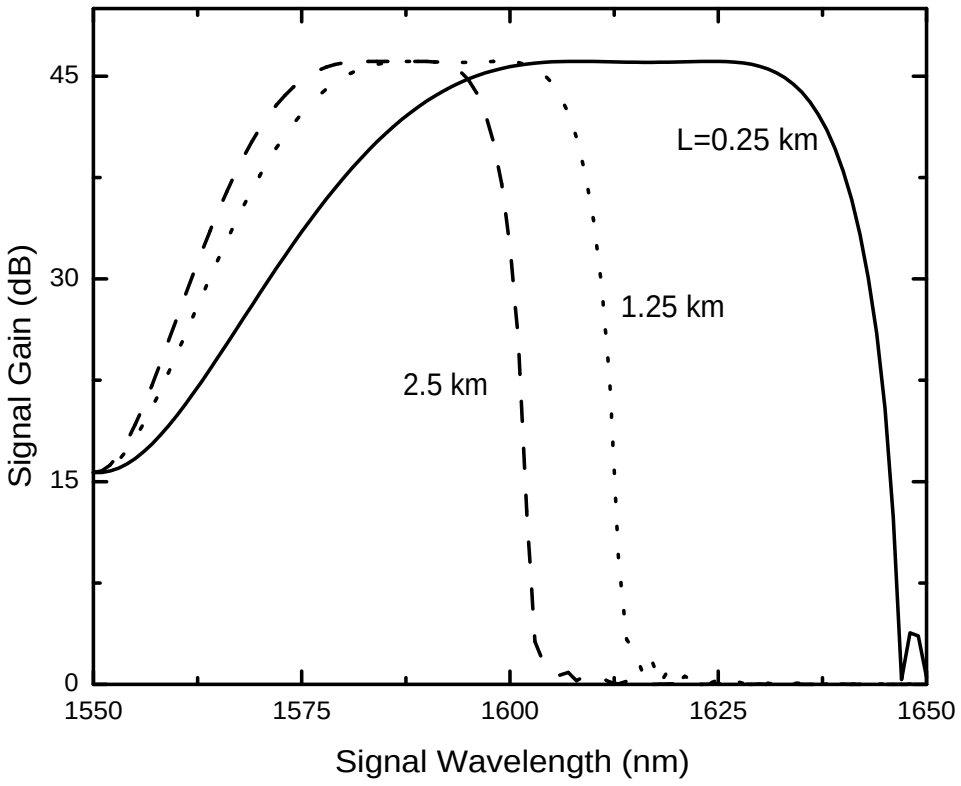

Figure 3 of Yaman et al.

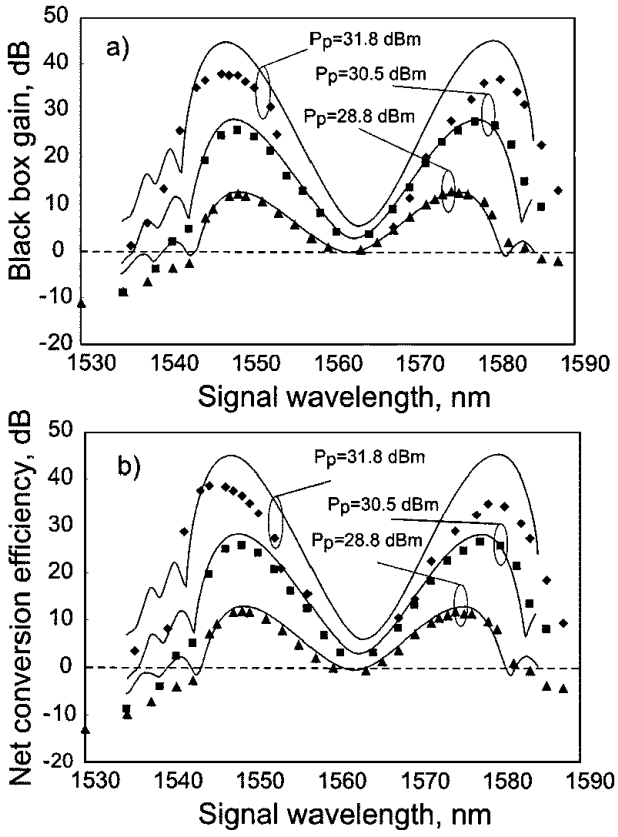

Figure 4 of Yaman et al.

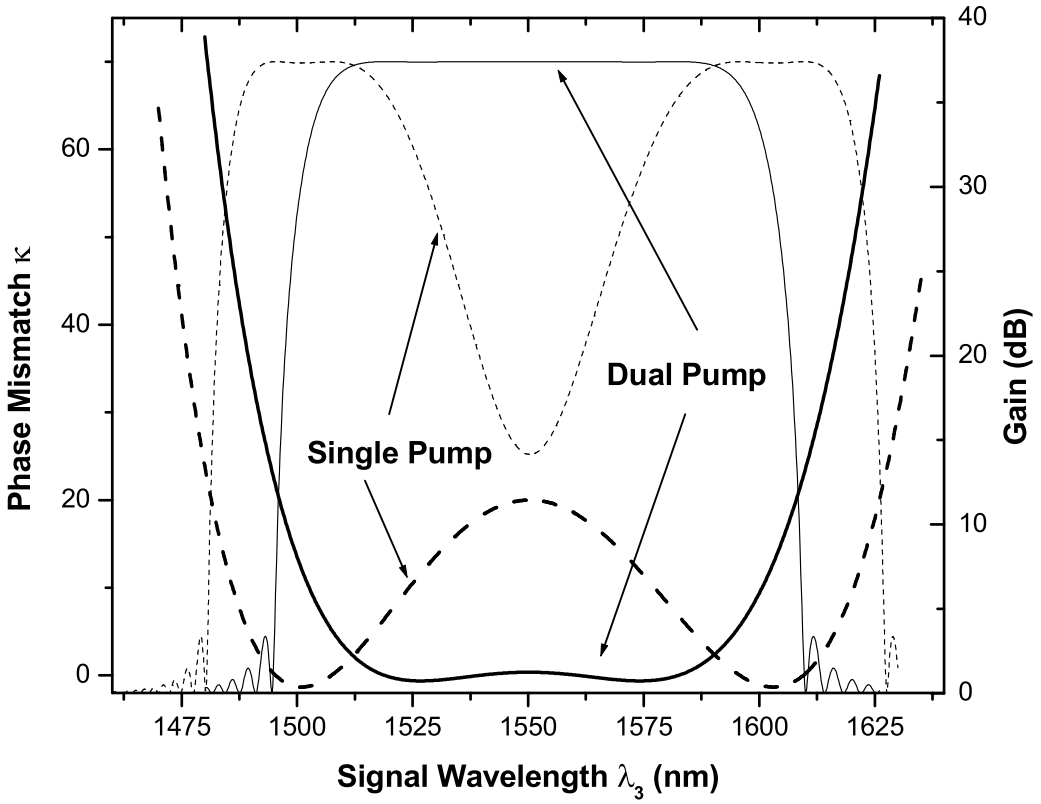

Figure 5 of Yaman et al.

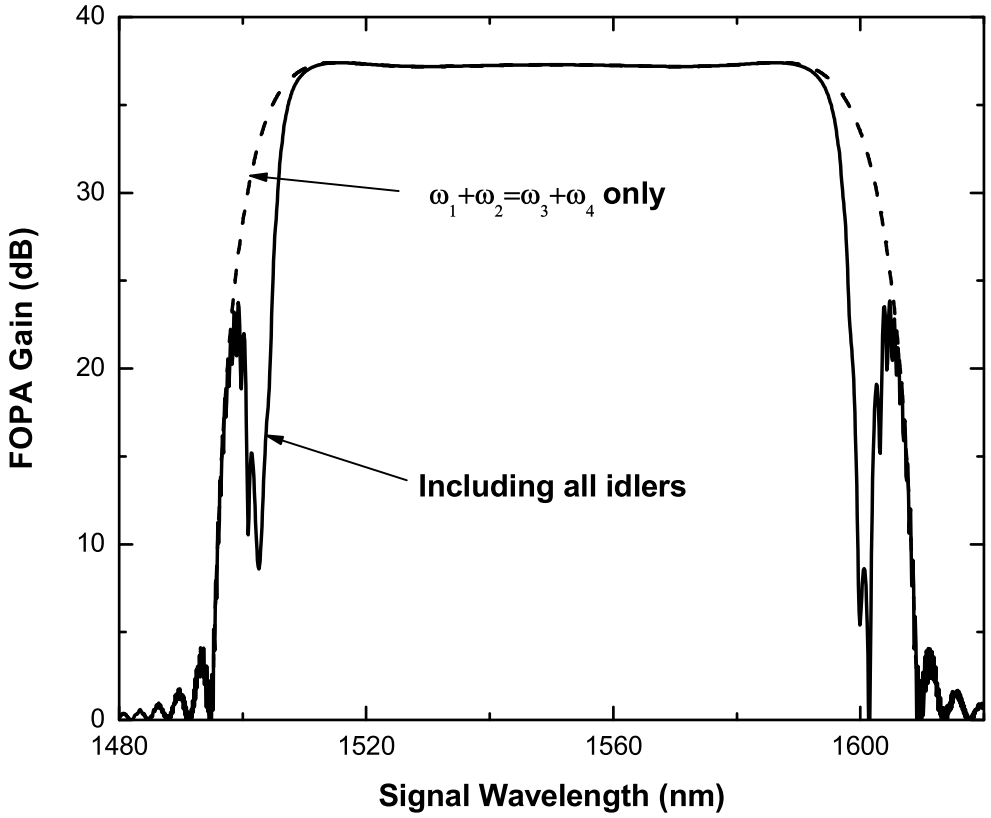

Figure 6 of Yaman et al.

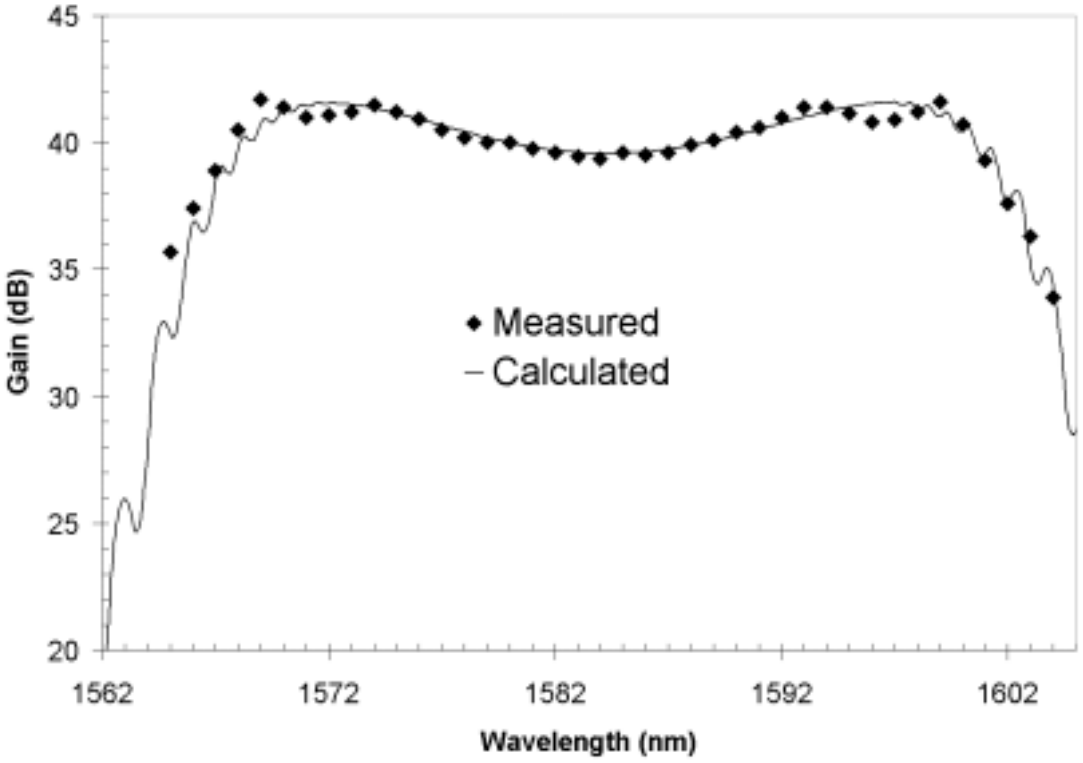

Figure 7 of Yaman et al.

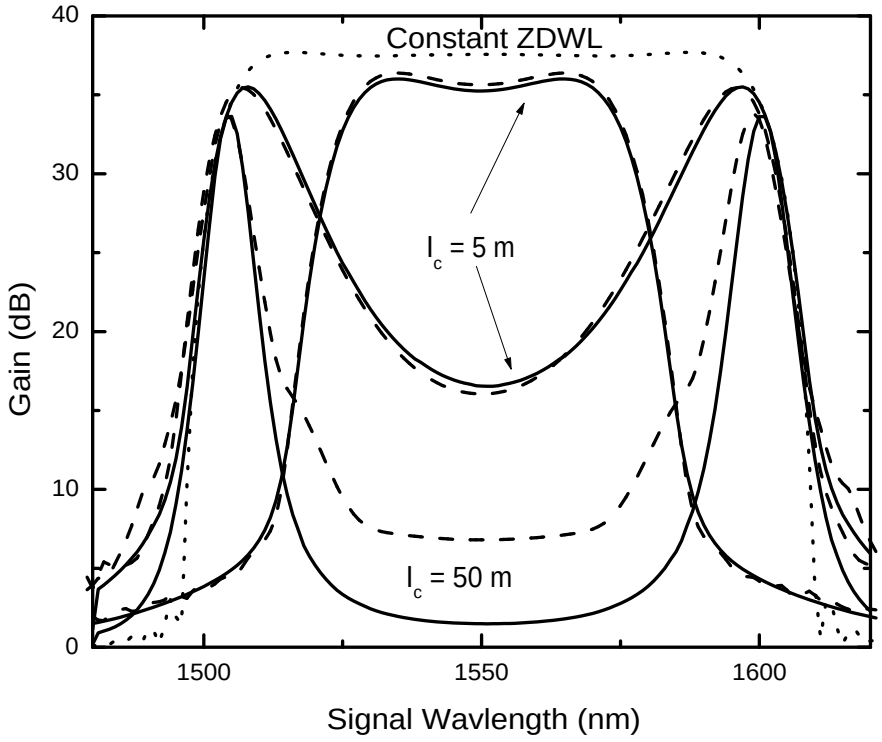

Figure 8 of Yaman et al.

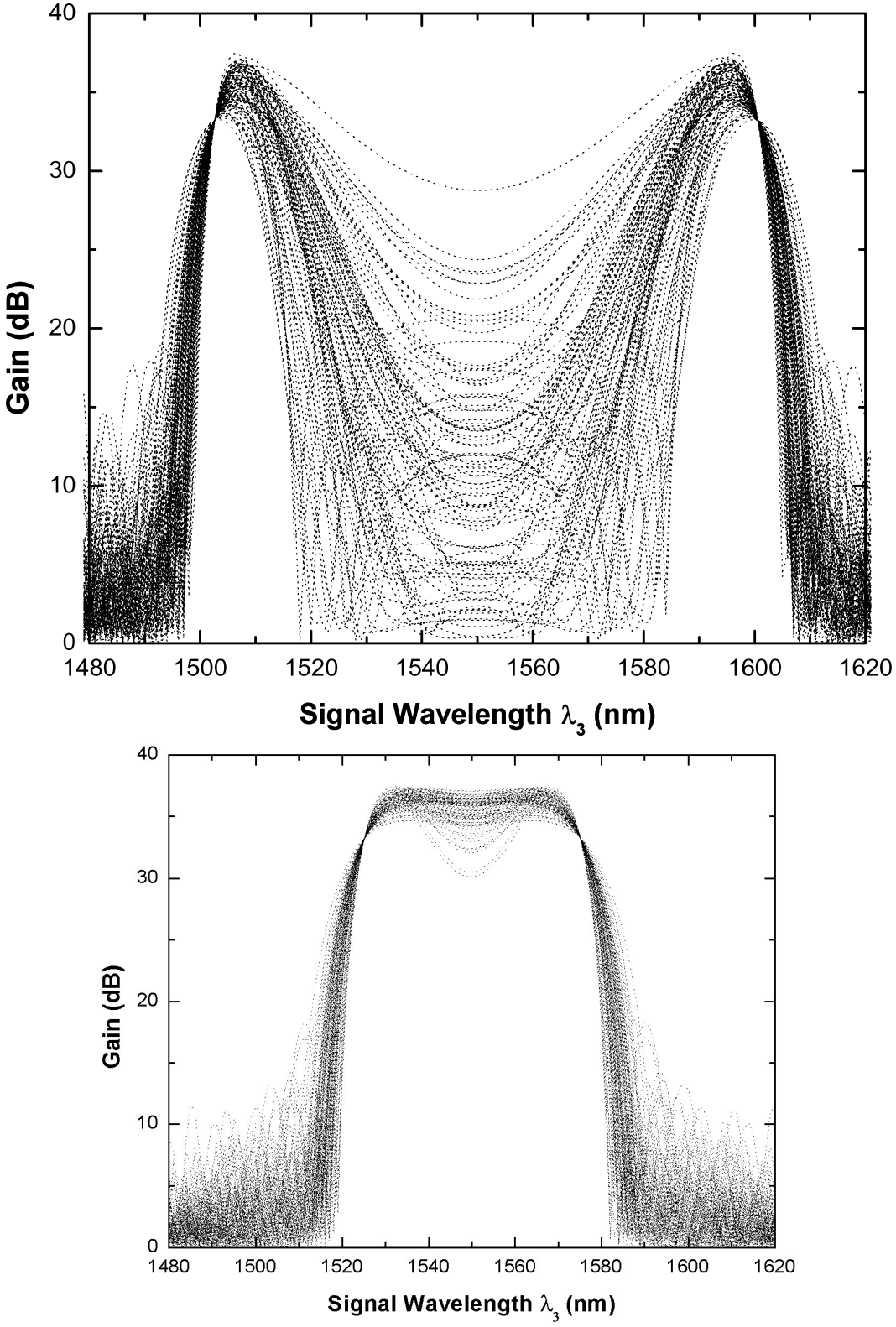

Figure 9 of Yaman et al.

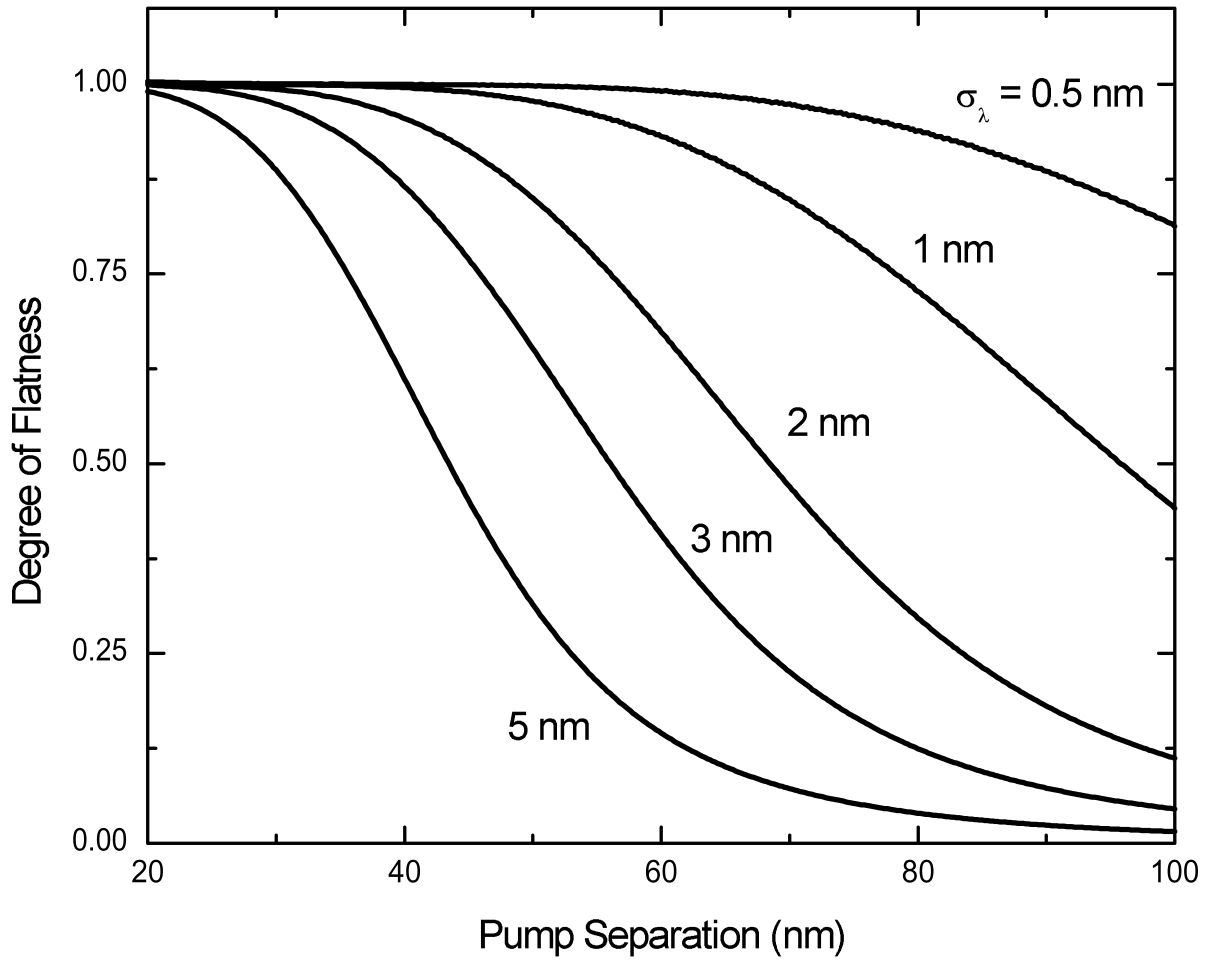

Figure 10 of Yaman et al.

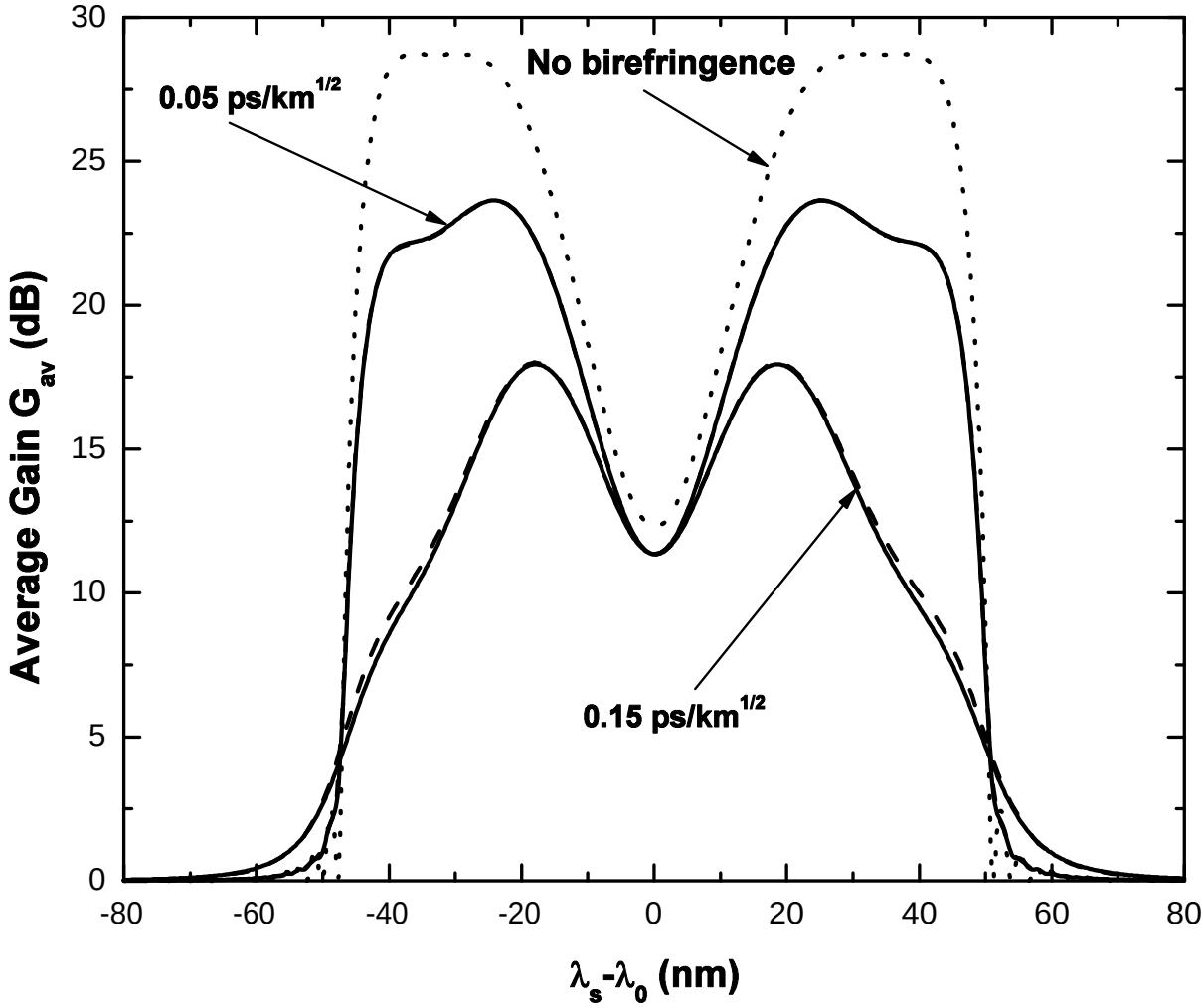

Figure 11 of Yaman et al.

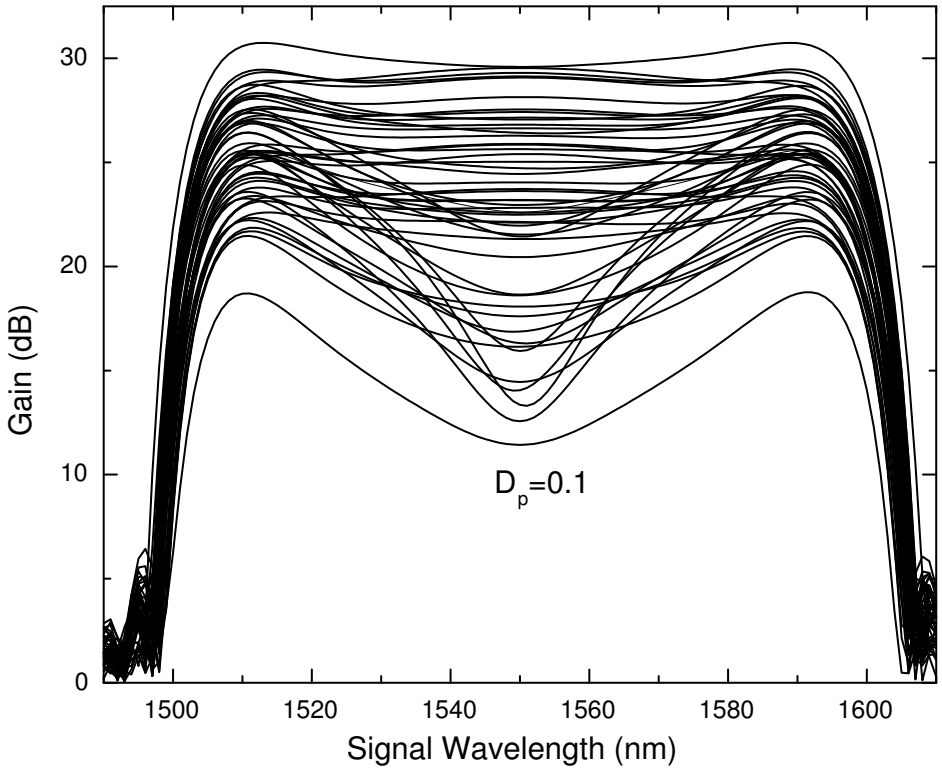

Figure 12 of Yaman et al.

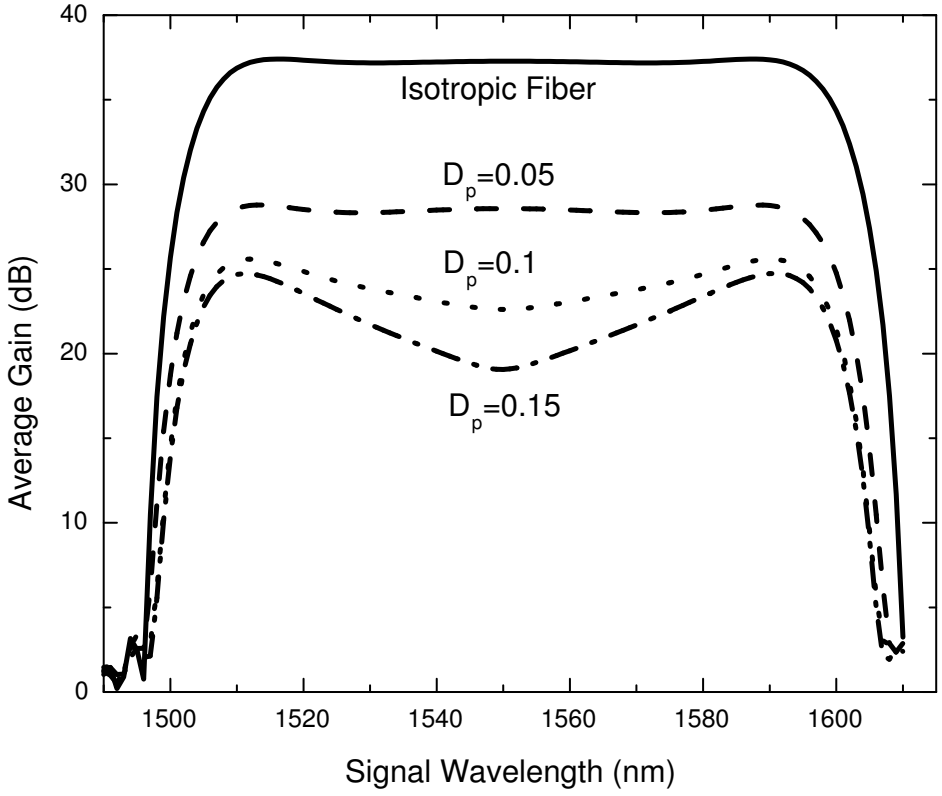

Figure 13 of Yaman et al.

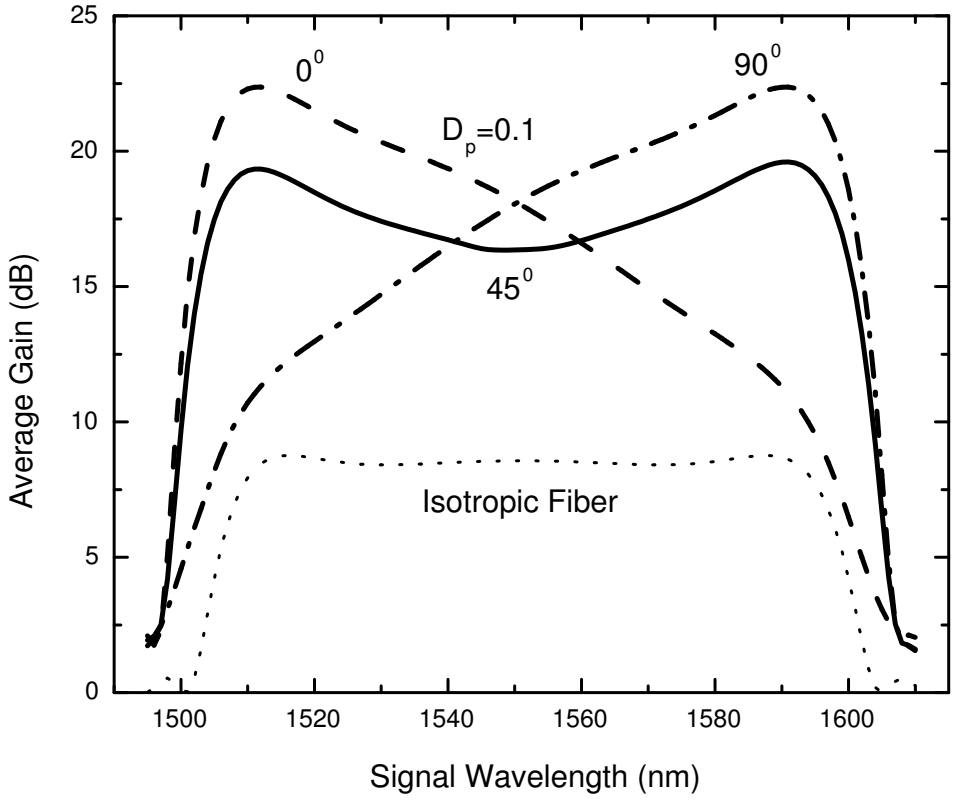

Figure 14 of Yaman et al.